

ISSN 2667-4211

ESKİŞEHİR TECHNICAL UNIVERSITY
JOURNAL OF SCIENCE AND TECHNOLOGY
A – Applied Sciences and Engineering

Volume **23** Number **2** - June - **2022**



Volume: 23 / Number: 2 / June - 2022

Eskiőehir Technical University Journal of Science and Technology A - Applied Sciences and Engineering (formerly Anadolu University Journal of Science and Technology A - Applied Sciences and Engineering) is an **peer-reviewed** and **refereed international journal** by Eskiőehir Technical University. Since 2000, it has been regularly published and distributed biannually and it has been published quarterly and **electronically only since 2016**.

Manuscripts submitted for publication are analyzed in terms of scientific quality, ethics and research methods in terms of its compliance by the Editorial Board representatives of the relevant areas. Then, the abstracts of the appropriate articles are sent to two different referees with a well-known in scientific area. If the referees agree to review the article, full text in the framework of the privacy protocol is sent. In accordance with the decisions of referees, either directly or corrected article is published or rejected. Confidential reports of the referees in the journal archive will be retained for ten years. All post evaluation process is done electronically on the internet. Detailed instructions to authors are available in each issue of the journal.

Eskiőehir Technical University holds the copyright of all published material that appear in Eskiőehir Technical University Journal of Science and Technology A - Applied Sciences and Engineering.

"Anadolu Üniversitesi Bilim ve Teknoloji Dergisi A - Uygulamalı Bilimler ve Mühendislik (Anadolu University Journal of Science and Technology A - Applied Sciences and Engineering)" published within Anadolu University started to be published within Eskiőehir Technical University which was established due to statute law 7141, in 2018. Hence, the name of the journal is changed to " Eskiőehir Technical University Journal of Science and Technology A - Applied Sciences and Engineering (Eskiőehir Teknik Üniversitesi Bilim ve Teknoloji Dergisi A - Uygulamalı Bilimler ve Mühendislik)".

Indexed by **DOAJ** - Directory of Open Access Journals, **EBSCO** and **ULAKBİM**



Volume: 23 / Number: 2 / June – 2022

Owner / Publisher: Prof. Dr. Tuncay DÖĐEROĐLU for Eskiőehir Technical University

EDITOR-IN-CHIEF

Prof. Dr. Murat TANIŐLI

Eskiőehir Technical University, Institute of Graduate Programs, 26470 Eskiőehir, TURKEY

Phone: +90-222-321 35 50 /**ext.:** 1755

Fax: +90-222 335 41 22

e-mail: mtanisli@eskisehir.edu.tr

CO-EDITOR IN CHIEF

Assoc. Prof. Dr. TuĐba ARAS

Eskiőehir Technical University, Institute of Graduate Programs, 26470 Eskiőehir, TURKEY

Phone: +90-222-321 35 50 /**ext.:** 1755

Fax: +90-222 335 41 22

e-mail: tugbasoganci@eskisehir.edu.tr

CONTACT INFORMATION

Eskiőehir Technical University Journal of Science and Technology

Eskiőehir Technical University, Institute of Graduate Programs, 26470 Eskiőehir, TURKEY

Phone: +90-222-321 35 50 /**ext.:** 1767

Fax: +90-222 335 41 22

e-mail : btada@eskisehir.edu.tr



Volume: 23 / Number: 2 / June - 2022

OWNER

Tuncay DÖĞEROĞLU, The Rector of Eskişehir Technical University

EDITORIAL BOARD

Murat TANIŞLI, Editor in Chief

Tuğba ARAS, Co-Editor in Chief

LANGUAGE EDITOR-ENGLISH

Hülya ALTUNTAŞ

SECTION EDITORS

-
- | | |
|--|--|
| Emin AÇIKKALP (ESTU, Turkey) | T. Hikmet KARAKOÇ (ESTU, Turkey) |
| Şener AĞALAR (ESTU, Turkey) | Onur KAYA (ESTU, Turkey) |
| Ziya AKÇA (Eskişehir Osmangazi University, Turkey) | Refail KASIMBEYLİ (ESTU, Turkey) |
| Haydar ARAS (Eskişehir Osmangazi University, Turkey) | Abidin KILIÇ (ESTU, Turkey) |
| Tuğba ARAS (ESTU) | Murat KILIÇ (ESTU, Turkey) |
| Funda ATEŞ (ESTU, Turkey) | Sabiha KOCA (Eskişehir Osmangazi University, Turkey) |
| Uğur AVDAN (ESTU, Turkey) | Mustafa KULAKÇI (ESTU, Turkey) |
| Nezihe AYAS (ESTU, Turkey) | Semra KURAMA (ESTU, Turkey) |
| Özge BAĞLAYAN (ESTU, Turkey) | Dilek Funda KURTULUŞ (METU, Turkey) |
| Recep BAKIŞ (ESTU, Turkey) | Anatoly NIKANOV (Saratov State Technical University, Slovenia) |
| Müfide BANAR (ESTU, Turkey) | Murad OMAROV (Kharkiv National University of Radio Electronics, Ukraine) |
| Ayşe H. BİLGE (Kadir Has University, Turkey) | Nuray ÖZASLAN (ESTU, Turkey) |
| Mehmet CANDAN (ESTU, Turkey) | Gürkan ÖZTÜRK (ESTU, Turkey) |
| Özgür CEYLAN (ESTU, Turkey) | Kadir Özgür PEKER (ESTU, Turkey) |
| Müjdat ÇAĞLAR (ESTU, Turkey) | Emrah PEKKAN (ESTU, Turkey) |
| Oğuzhan ÇAĞLAYAN (Bilecik Şeyh Edebali University, Turkey) | Najeeb REHMAN (Comsat University, Pakistan) |
| Yunus Ali ÇENGEL (Adnan Menderes University, Turkey) | İsmail Hakkı SARPÜN (Akdeniz University, Turkey) |
| Hakan ÇEVİKALP (Eskişehir Osmangazi University, Turkey) | Uğur SERİNCAN (ESTU, Turkey) |
| Rasime DEMİREL (ESTU, Turkey) | Cem SEVİK (ESTU, Turkey) |
| Sedef DİKMEN (ESTU, Turkey) | İlkin YÜCEL ŞENGÜN (Ege University, Turkey) |
| Faruk DİRİSAĞLUK (Eskişehir Osmangazi University) | Sevil ŞENTÜRK (ESTU, Turkey) |
| Barış ERBAŞ (ESTU, Turkey) | Aynur ŞENSOY ŞORMAN (ESTU, Turkey) |
| Ömer Nezih GEREK (ESTU, Turkey) | Engin TIRAŞ (ESTU, Turkey) |
| Özer GÖK (ESTU, Turkey) | Ümran Tezcan ÜN (ESTU, Turkey) |
| Emrah GÖKALTUN (ESTU, Turkey) | Önder TURAN (ESTU, Turkey) |
| Serdar GÖNCÜ (ESTU, Turkey) | Muammer TÜN (ESTU, Turkey) |
| Zerrin AŞAN GREENACRE (ESTU, Turkey) | Gülşay ÜNAL (ESTU, Turkey) |
| Cihan KALELİ (ESTU, Turkey) | Gülgün YILMAZ ÜNAL (ESTU, Turkey) |
| Gordona KAPLAN (ESTU, Turkey) | |
| Alpagut KARA (ESTU, Turkey) | |
-

Secretary/Typset

Handan YİĞİT



ABOUT

Eskişehir Technical University Journal of Science and Technology A - Applied Sciences and Engineering (formerly Anadolu University Journal of Science and Technology A - Applied Sciences and Engineering) is an peer-reviewed and refereed international journal by Eskişehir Technical University. Since 2000, it has been regularly published and distributed biannually and it has been published quarterly and electronically only since 2016.

- **The journal accepts only ENGLISH language manuscripts.**
- **The journal is indexed by EBSCO, DOAJ and ULAKBIM.**

AIM AND SCOPE

The journal publishes high quality original research papers in the field of engineering and applied science. Special Issues devoted to important topics in science and technology will occasionally be published. The journal publishes research papers in the fields of applied science and technology such as Physics, Biology, Mathematics, Statistics, Chemistry and Chemical Engineering, Environmental Sciences and Engineering, Civil Engineering, Earth and Atmospheric Sciences, Electrical and Electronical Engineering, Computer Science and Informatics, Materials Sciences and Engineering, Mechanical Engineering, Mining Engineering, Industrial Engineering, Aeronautics and Astronautics, Health Sciences, Pharmaceutical Sciences, and so on.

PEER REVIEW PROCESS

Manuscripts are first reviewed by the editorial board in terms of its its journal's style rules scientific content, ethics and methodological approach. If found appropriate, the manuscript is then send to at least two renown referees by editor. The decision in line with the referees may be an acceptance, a rejection or an invitation to revise and resubmit. Confidential review reports from the referees will be kept in archive. All submission process manage through the online submission systems.

OPEN ACCESS POLICY

This journal provides immediate open access to its content on the principle that making research freely available to the public supports a greater global exchange of knowledge. Copyright notice and type of licence : **CC BY-NC-ND**.

The journal doesn't have Article Processing Charge (APC) or any submission charges.

ETHICAL RULES

You can reach the Ethical Rules in our journal in full detail from the link below:

<https://dergipark.org.tr/tr/pub/estubtda/page/10202>

AUTHOR GUIDELINES

All manuscripts must be submitted electronically.

You will be guided stepwise through the creation and uploading of the various files. There are no page charges. Papers are accepted for publication on the understanding that they have not been published and are not going to be considered for publication elsewhere. Authors should certify that neither the manuscript nor its main contents have already been published or submitted for publication in another journal. We ask a signed **Copyright Form** to start the evaluation process. After a manuscript has been submitted, it is not possible for authors to be added or removed or for the order of authors to be changed. If authors do so, their submission will be cancelled.

Manuscripts may be rejected without peer review by the editor-in-chief if they do not comply with the instructions to authors or if they are beyond the scope of the journal. After a manuscript has been accepted for publication, i.e. after referee-recommended revisions are complete, the author will not be permitted to make any changes that constitute departures from the manuscript that was accepted by the editor. Before publication, the galley proofs are always sent to the authors for corrections. Mistakes or omissions that occur due to some negligence on our part during final printing will be rectified in an errata section in a later issue.

This does not include those errors left uncorrected by the author in the galley proof. The use of someone else's ideas or words in their original form or slightly changed without a proper citation is considered plagiarism and will not be tolerated. Even if a citation is given, if quotation marks are not placed around words taken directly from another author's work, the author is still guilty of plagiarism. All manuscripts received are submitted to iThenticateR, a plagiarism checking system, which compares the content of the manuscript with a vast database of web pages and academic publications. Manuscripts judged to be plagiarised or self-plagiarised, based on the iThenticateR report or any other source of information, will not be considered for publication.

CONFLICT OF INTEREST STATEMENT

The authors are obliged to present the conflict of interest statement at the end of the article.

Preparation of Manuscript

Style and Format: Manuscripts should be **single column** by giving one-spaced with 2.5-cm margins on all sides of the page, in Times New Roman font (font size 11). Every page of the manuscript, including the title page, references, tables, etc., should be numbered. All copies of the manuscript should also have line numbers starting with 1 on each consecutive page.

Manuscripts must be upload as word document (*.doc, *.docx vb.). Please avoid uploading texts in *.pdf format.

Manuscripts should be written in English.

Symbols, Units and Abbreviations: Standard abbreviations and units should be used; SI units are recommended. Abbreviations should be defined at first appearance, and their use in the title and abstract should be avoided. Generic names of chemicals should be used. Genus and species names should be typed in italic or, if this is not available, underlined.

Please refer to equations with capitalisation and unabbreviated (e.g., as given in Equation (1)).

Manuscript Content: Articles should be divided into logically ordered and numbered sections. Principal sections should be numbered consecutively with Arabic numerals (1. Introduction, 2. Formulation of problem, etc.) and subsections should be numbered 1.1., 1.2., etc. Do not number the Acknowledgements or References sections. The text of articles should be, if possible, divided into the following sections: Introduction, Materials and Methods (or Experimental), Results, Discussion, and Conclusion.

Title and contact information

The first page should contain the full title in sentence case (e.g., Hybrid feature selection for text classification), the full names (last names fully capitalised) and affiliations (in English) of all authors (Department, Faculty, University, City, Country, E-mail), and the contact e-mail address for the clearly identified corresponding author.

Abstract

The abstract should provide clear information about the research and the results obtained, and should not exceed 300 words. The abstract should not contain citations and must be written in Times New Roman font with font size 9.

Keywords

Please provide 3 to 5 keywords which can be used for indexing purposes.

Introduction

The motivation or purpose of your research should appear in the “Introduction”, where you state the questions you sought to answer, and then provide some of the historical basis for those questions.

Methods

Provide sufficient information to allow someone to repeat your work. A clear description of your experimental design, sampling procedures, and statistical procedures is especially important in papers describing field studies, simulations, or experiments. If you list a product (e.g., animal food, analytical device), supply the name and location of the manufacturer. Give the model number for equipment used.

Results

Results should be stated concisely and without interpretation.

Discussion

Focus on the rigorously supported aspects of your study. Carefully differentiate the results of your study from data obtained from other sources. Interpret your results, relate them to the results of previous research, and discuss the implications of your results or interpretations.

Conclusion

This should state clearly the main conclusions of the research and give a clear explanation of their importance and relevance. Summary illustrations may be included.

Acknowledgments

Acknowledgments of people, grants, funds, etc. should be placed in a separate section before the reference list. The names of funding organizations should be written in full.

Conflict of Interest Statement

The authors are obliged to present the conflict of interest statement at the end of the article after the acknowledgments section.

References

Citations in the text should be identified by numbers in square brackets. The list of references at the end of the paper should be given in order of their first appearance in the text or in alphabetical order according to the surname of the first author. All authors should be included in reference lists unless there are 10 or more, in which case only the first 10 should be given, followed by 'et al.'. Do not use individual sets of square brackets for citation numbers that appear together, e.g., [2, 3, 5–9], not [2], [3], [5]–[9]. Do not include personal communications, unpublished data, websites, or other unpublished materials as references, although such material may be inserted (in parentheses) in the text. In the case of publications in languages other than English, the published English title should be provided if one exists, with an annotation such as "(article in Turkish with an abstract in English)". If the publication was not published with an English title, cite the original title only; do not provide a self-translation. References should be formatted as follows (please note the punctuation and capitalisation):

Journal articles

Journal titles should be abbreviated according to ISI Web of Science abbreviations.

Guyon I and Elisseeff A. An introduction to variable and feature selection. *J Mach Learn Res*, 2003; 3: 1157-1182.

Izadpanahi S, Ozcinar C, Anbarjafari G and Demirel H. Resolution enhancement of video sequences by using discrete wavelet transform and illumination compensation. *Turk J Elec Eng & Comp Sci*, 2012; 20: 1268-1276.

Books

Haupt RL and Haupt SE. *Practical Genetic Algorithms*. 2nd ed. New York, NY, USA: Wiley, 2004.

Kennedy J and Eberhart R. *Swarm Intelligence*. San Diego, CA, USA: Academic Press, 2001.

Chapters in books

Poore JH, Lin L, Eschbach R and Bauer T. Automated statistical testing for embedded systems. In: Zander J, Schieferdecker I, Mosterman PJ, editors. *Model-Based Testing for Embedded Systems*. Boca Raton, FL, USA: CRC Press, 2012. pp. 111-146.

Conference proceedings

Li RTH and Chung SH. Digital boundary controller for single-phase grid-connected CSI. In: *IEEE 2008 Power Electronics Specialists Conference*; 15–19 June 2008; Rhodes, Greece. New York, NY, USA: IEEE. pp. 4562-4568.

Theses

Boynukalın Z. Emotion analysis of Turkish texts by using machine learning methods. MSc, Middle East Technical University, Ankara, Turkey, 2012.

Tables and Figures

All illustrations (photographs, drawings, graphs, etc.), not including tables, must be labelled “Figure.” Figures must be submitted in the manuscript.

All tables and figures must have a caption and/or legend and be numbered (e.g., Table 1, Figure 2), unless there is only one table or figure, in which case it should be labelled “Table” or “Figure” with no numbering. Captions must be written in sentence case (e.g., Macroscopic appearance of the samples.). The font used in the figures should be Times New Roman with 9 pt. If symbols such as \times , μ , η , or ν are used, they should be added using the Symbols menu of Word.

All tables and figures must be numbered consecutively as they are referred to in the text. Please refer to tables and figures with capitalisation and unabbreviated (e.g., “As shown in Figure 2...”, and not “Fig. 2” or “figure 2”).

The resolution of images should not be less than 118 pixels/cm when width is set to 16 cm. Images must be scanned at 1200 dpi resolution and submitted in jpeg or tiff format. Graphs and diagrams must be drawn with a line weight between 0.5 and 1 point. Graphs and diagrams with a line weight of less than 0.5 point or more than 1 point are not accepted. Scanned or photocopied graphs and diagrams are not accepted.

Figures that are charts, diagrams, or drawings must be submitted in a modifiable format, i.e. our graphics personnel should be able to modify them. Therefore, if the program with which the figure is drawn has a “save as” option, it must be saved as *.ai or *.pdf. If the “save as” option does not include these extensions, the figure must be copied and pasted into a blank Microsoft Word document as an editable object. It must not be pasted as an image file (tiff, jpeg, or eps) unless it is a photograph.

Tables and figures, including caption, title, column heads, and footnotes, must not exceed 16 × 20 cm and should be no smaller than 8 cm in width. For all tables, please use Word’s “Create Table” feature, with no tabbed text or tables created with spaces and drawn lines. Please do not duplicate information that is already presented in the figures.

CONTENTS

RESEARCH ARTICLE

INVESTIGATION OF MICROALGAE GASIFICATION UNDER STEAM ATMOSPHERE IN DOWNDRAFT GASIFIER BY USING ASPEN PLUS® <i>B. Kekik, U. Özveren</i>	149
THE DETECTION OF EGGHELL CRACKS USING DIFFERENT CLASSIFIERS <i>M. Yumurtacı, Z. Balcı, S. Ergin, İ. Yabanova</i>	161
SOLAR ENERGY ASSISTS SEDIMENT MICROBIAL FUEL CELL TO GENERATE GREEN ENERGY FROM LIQUID ORGANIC WASTE <i>O. C. Türker</i>	173
PREDICTING MYOCARDIAL INFARCTION COMPLICATIONS AND OUTCOMES WITH DEEP LEARNING <i>İ. B. Yavru, S. Yılmaz Gündüz</i>	184



RESEARCH ARTICLE

INVESTIGATION OF MICROALGAE GASIFICATION UNDER STEAM ATMOSPHERE IN
DOWNDRAFT GASIFIER BY USING ASPEN PLUS®

Berna KEKİK¹  and Uğur ÖZVEREN^{2,*} 

^{1,2*} Chemical Engineering Department, Faculty of Engineering, Marmara University, Istanbul, Turkey

ABSTRACT

Energy production faces environmental and economic problems due to growing population and fossil fuel uncertainty. These concerns have led researchers to find a widely available and renewable alternative such as biomass instead of fossil fuels. Microalgae is one of the most promising biofuels because it grows quickly and has a higher calorific value. Steam gasification is an alternative method to convert biomass into syngas with higher H₂ content and lower CO₂ content compared to other thermochemical conversion processes. In the present work, the downdraft gasifier model was developed using Aspen Plus® simulation software, which is capable of investigating the performance of microalgae gasification. Prior to the gasification performance evaluation, the validity of the model was tested with the results of an experimental study conducted with a different feedstock. The validation of the model was successfully completed, and it was found that the initial gas compositions of H₂, CO₂, CO and CH₄ were very similar between the experimental study and the developed model. The effects of the main process parameters, such as the steam/biomass ratio and the gasification temperature, on the syngas composition and the higher heating value (HHV) of the syngas were evaluated. The results obtained with Aspen Plus® showed that increasing the temperature had a great effect on the H₂ and CO composition of the syngas. They increased from 50.72% to 56.47% and from 28.11% to 28.84%, respectively. The simulation results also showed that the increasing S/B ratio favored the steam-related reactions and increased the H₂ content in the syngas. However, a decreasing trend in CH₄ content also decreased the HHV of the syngas as a function of temperature and steam.

Keywords: Gasification; Biomass; Microalgae; Downdraft Gasifier; Aspen Plus®

1. INTRODUCTION

Enlarging energy demand due to the growing population causes considerable economic problems and global climate change [1, 2]. Renewable sources provide a more sustainable and economical method to prevent the detrimental effect of fossil fuels on energy production [3]. Fossil fuel consumption needs to be reduced and its application methods must be changed because of the emissions of carbon dioxide (CO₂) [4]. Biomass is considered a carbon-neutral feedstock that can substitute fossil fuels [5, 6]. Microalgae, as the third-generation biomass feedstock, efficiently capture CO₂ [7] through photosynthetic recirculation and are used for synthetic fuel via various conversion processes such as biochemical [8], hydrothermal [9], combustion [10], thermochemical [11, 12]. Thermochemical conversion of microalgae is seen as more preferable to biochemical conversion because the biochemical process needs a longer reaction time and has less conversion efficiency than thermochemical processes [13]. Furthermore, the use of microalgae does not compete with traditional food crops. Therefore, microalgae is a very promising feedstock for thermochemical conversion methods because of their high growth rate (up to 20 g dry algae per m² per day) and widespread availability [14].

The increasing desire to promote the use of biomass as a renewable energy source is giving new momentum to the development of gasification technologies. Gasification is one of the most favorable thermochemical routes that produces syngas mostly composed of methane (CH₄), carbon monoxide

(CO), hydrogen (H₂), and CO₂ with varying characteristics can be obtained by altering the feedstock [15, 16]. Gasification under steam atmosphere is gaining momentum as it can obtain high-quality syngas [17] at a relatively low operating expense. Moreover, it can generate more H₂ yield than all the gasification agents (air, O₂, CO₂) [18].

The syngas composition can be varied concerning the physicochemical structure of fuel, operational conditions of the gasification process, and gasifier type [19]. The downdraft gasifier is a common technique for biomass gasification among the present three types of gasifiers [20]. Related to capacity and feedstock type, the downdraft gasifier is one of the fixed bed gasifiers and is the most compatible type due to its low construction cost, low tar content in syngas, and simpler and more compact design compared with the entrained and fluidized bed reactors [21, 22].

The modeling and simulation of downdraft gasifier performance by using simulation tools like an equation-driven simulation program based on mass and energy balance are valuable for better gasifier design [23]. Aspen Plus® is one of the most popular equation-oriented simulation programs that can make successful thermodynamic approaches in line with mathematical models to simulate the biomass gasification process more healthily, saving time and money is a very common technology today [24–26]. The optimization of the syngas composition and the obtained syngas with the desired quality are the most important concerns in gasification. Investigation of the optimal values of the gasification parameters like pressure, gasification temperature, and amount of gasifying agent is conducted in the Aspen Plus® program very fast and reliably. On the other hand, there are a few studies for the modeling of downdraft gasifiers by using Aspen Plus® [27, 28].

In this study, we elucidated the HHV and syngas composition of microalgae gasification under steam atmosphere from a downdraft gasifier by using Aspen Plus®. The results and adopted method in this paper give a point of reference to properly designing downdraft gasifiers for high-valued gasifier products.

2. METHODS

2.1. Sample Characterization

The microalgae as a marine biomass sample were chosen as a feedstock in this study, and the physicochemical properties of it were taken from the biomass database of ECN [29]. Microalgae do not have a stem, root, and leave like plants, however it uses CO₂, sunlight, and water to grow. Depending on their growth status and species, microalgae generally consist of protein (20–50%), lipid (9.5–42%), and carbohydrate (17–57%) [30]. According to the energetic characteristics, the microalgae sample that had a HHV (dry basis) of 23.48 MJ/kg was preferred for the gasification process. The ultimate and proximate analysis results of the microalgae are given in Table 1. The nitrogen, sulfur, hydrogen and carbon content of microalgae were determined experimentally, whereas oxygen content was calculated by difference.

Table 1. Proximate and ultimate analyses results of the microalgae sample

<i>Proximate Analysis (dry basis)</i>	<i>Value (wt.%)</i>
<i>Fixed Carbon</i>	15.68
<i>Volatile Matter</i>	81.80
<i>Ash</i>	2.52
<i>Moisture Content</i>	5.22
<i>Ultimate Analysis (dry basis)</i>	<i>Value (wt.%)</i>
<i>Carbon</i>	52.73
<i>Oxygen</i>	29.03
<i>Sulphur</i>	0.49
<i>Hydrogen</i>	7.22
<i>Nitrogen</i>	8.01

2.2. Downdraft Gasifier Model

Aspen Plus[®] is an equation-oriented program that is used to simulate several chemical, physical and biological processes based on phase equilibrium and energy and mass balances [23]. Aspen Plus[®] software is preferred by many researchers and industrial facilities instead of experimental studies due to its high capability to measure and examine operating parameters and analyze system performance in a very short time. Aspen Plus[®] has a wide database for calculation of physical properties of streams and components. Another advantage of Aspen Plus[®] is that solid components such as biomass, coal can be correctly handled in the well-designed model for gasification applications [31, 32]. The steady-state and equilibrium-based model of the downdraft gasifier for microalgae gasification has been developed using Aspen Plus[®] V11 [33]. The flow chart of the downdraft gasifier in the Aspen Plus[®] software was presented in Figure 1.

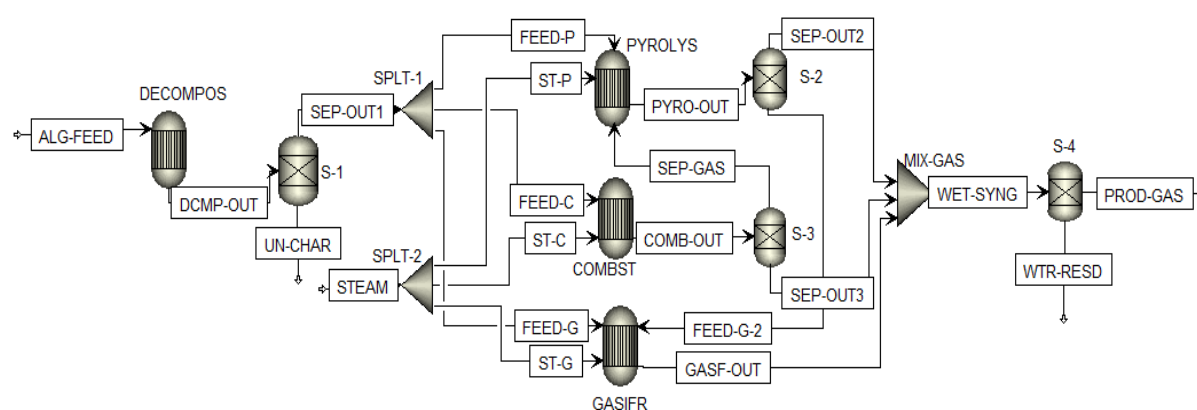


Figure 1. Flowsheet of the downdraft gasifier model

The Soave-Redlich-Kwong (SRK) that is recommended by the Aspen Plus[®] user manual for this type of application has been selected as the equation of state to determine the physical properties of the conventional components with STEAMNBS as the free-water method. The property methods have been selected as DCOALIGT and HCOALGEN to calculate density and enthalpy values, respectively for biomass as a nonconventional component [34]. The components which are possible to be formed as a result of gasification steps have been identified in the Aspen Plus[®] database.

In a downdraft gasifier, many complex reactions can occur, but they cannot be simulated with a zero-dimensional model, thus the main parts of gasification have been simulated considering some assumptions as mentioned below:

- The gasification system is operated in a steady state.
- The entire system is isothermal.
- There is no pressure drop in streams and blocks.
- All reactions reach chemical equilibrium and occur fast.
- Ash is considered an inert material and does not contribute to the reaction.
- Char consists of only carbon.
- Heavy hydrocarbons are omitted from the syngas composition.

Three Gibbs reactors have been used to simulate the pyrolysis, combustion, and gasification parts of the downdraft gasifier. Gibbs reactors work based on Gibbs free energy minimization principle, this method is also called non-stoichiometric and any information about the reaction steps and conversion rates are not needed to model reactors [35].

The blocks and reactors have been selected and formed the downdraft gasifier model. The microalgae has been defined as nonconventional solid and fed to the system, then decomposition, pyrolysis, and gasification steps have occurred consecutively. Water and other residual components have been separated and syngas containing H₂, CO, CH₄, and CO₂ has been produced.

3. RESULTS

3.1. Model Validation

Before investigating the performance of this model for the selected microalgae, the accuracy of the developed downdraft gasifier model should be validated with the experimental study. For the model validation, a gasification system was performed in the same condition as the experimental study that was selected from the literature. The syngas composition was compared for H₂, CO, CH₄, and CO₂. The results of the comparison of the model and the literature study were presented with the operational conditions in Table 2.

Table 2. Comparison of experimental and model results

Sample	Karanja Press Seed Cake	
Gasification Temperature	800 °C	
Gasification Pressure	1 atm	
Syngas Composition (%v/v.dry)	Experimental [36]	Model
H ₂	37.26	37.92
CO	48.70	50.93
CO ₂	4.20	4.29
CH ₄	2.3	4.42

In the experimental work [36], Karanja Press Seed Cake was selected as the feedstock, and the experiment was conducted under atmospheric pressure with the gasification temperature at 800 °C. Working conditions and feedstock in the experimental study were defined identically to the Aspen Plus[®] model. Comparison of results depicts that the H₂, CO, and CO₂ compositions were obtained with a small difference. The deviation in CH₄ composition between the model and the experimental study can be explained with some assumptions and calculations of the Gibbs reactors in the Aspen Plus[®] model. Unlike the model that works based on the chemical equilibrium in the real case, conversion rates of the reaction depend on the kinetics and residence time. This situation was discussed by some researchers who studied it with the equilibrium model [26, 37-39]. Hereby, the validation of the downdraft gasifier model was completed successfully, and the newly developed model was found to be reasonably acceptable.

3.2. Parametric Study

The gasification properties of microalgae under a steam atmosphere in terms of HHV of syngas and gas composition were investigated according to change of gasification temperature and steam/biomass ratio (S/B) by using the sensitivity analysis tool in Aspen Plus[®].

3.2.1. Investigation of gasification temperature on syngas composition

Temperature is one of the key parameters that influences the syngas composition due to temperature promoted endothermic and exothermic reactions. As shown in Figure 2, the change of the syngas composition with respect to gasification temperature varied between 600-1000 °C while the S/B ratio was kept constant at 1.5.

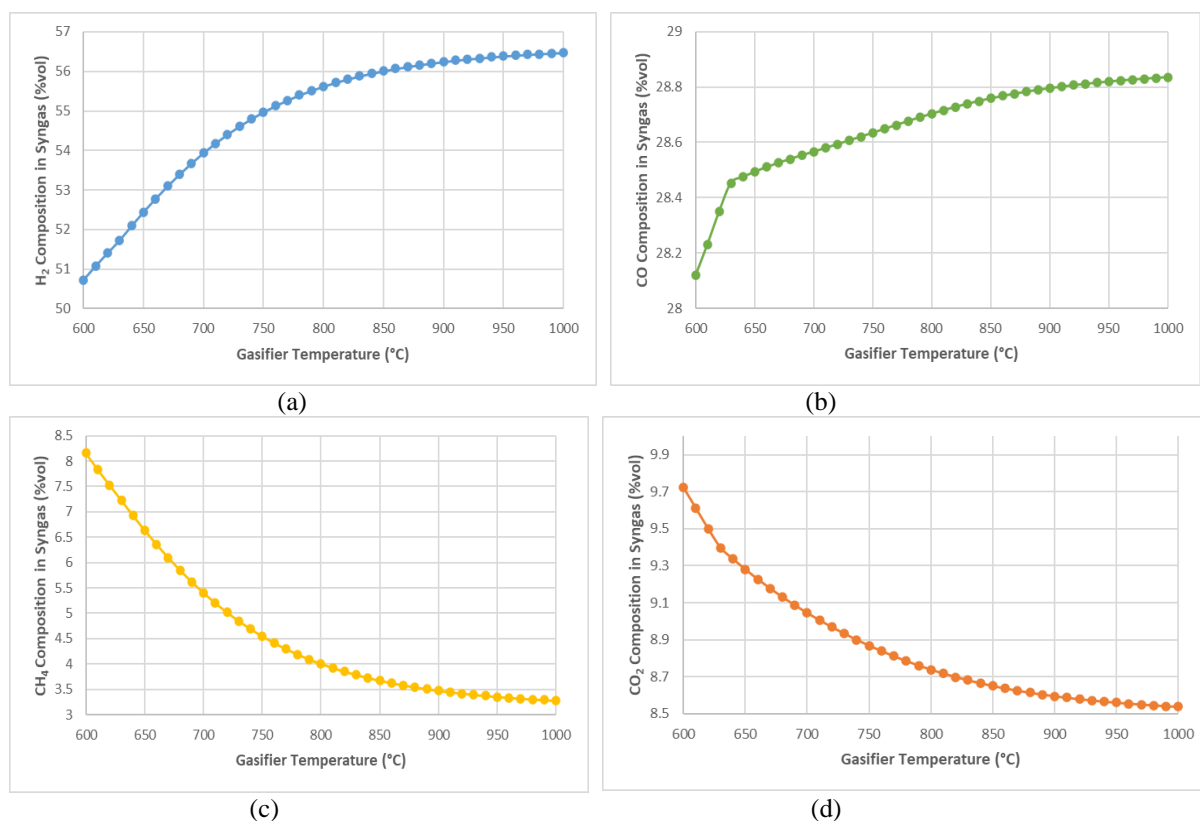


Figure 2. Effect of the temperature on syngas composition (a) H₂, (b) CO, (c) CH₄, (d) CO₂

In general, solid fuel decomposes effectively and a higher amount of syngas is produced at relatively higher temperatures [24]. As illustrated in Figure 2.a, the H₂ content in syngas rises sharply between 600 and 800 °C but the increase continues slower after the temperature point at 800 °C. While the temperature reached 1000 °C, the H₂ content fluctuated between 50.72% and 56.47%. The change of CO content in syngas showed a similar trend to H₂ and it increased from 28.11% to 28.84% at a temperature between 600-1000 °C as seen in Figure 2.b. These trends can be explained by endothermic reactions such as heterogenous, water-gas ($C + H_2O \leftrightarrow CO + H_2$) and gas phase, steam-methane reforming ($CH_4 + H_2O \leftrightarrow CO + 3H_2$). The percentage increase in H₂ is higher than in CO because of the stoichiometric coefficients of H₂ in the reactions. Furthermore, a reverse trend of the CO and CO₂ can be explained by the Boudouard reaction ($C + CO_2 \leftrightarrow 2CO$) that occurs in the downdraft gasifier after the temperature of 800 °C. The decreasing behavior was observed in the CH₄ and CO₂ contents in syngas while the temperature increased in the same range. Considering all these endothermic reactions, the tendency of the components showed good agreement with the literature studies based on Le Chatelier's principle which states that high temperatures shift the reaction side to products. However, exothermic reactions approach the reactant side [32, 40-42]. The desired components which are H₂ and CO in the gasifier increased significantly until the temperature reached 800 °C, after that point the increase continued very slowly. Taking into account the energy consumption, the optimum gasifier temperature was determined as 800 °C.

3.2.2. Investigation of gasification temperature on HHV of syngas

The higher heating value (HHV) states the heat produced from the combustion of the unit mass or volume of syngas [43]. The combustible characteristics of the syngas vary depending on the calorific values of each component and the syngas composition accordingly. Thus, the HHV is an important

criterion for evaluating the quality of the syngas [44]. The HHV of syngas can be provided from the property sets section as stream properties in Aspen Plus[®] program without needing extra calculation. The influence of gasification temperature on the HHV of syngas was investigated at the same temperature range as the syngas composition and sensitivity analysis results are presented in Figure 3.

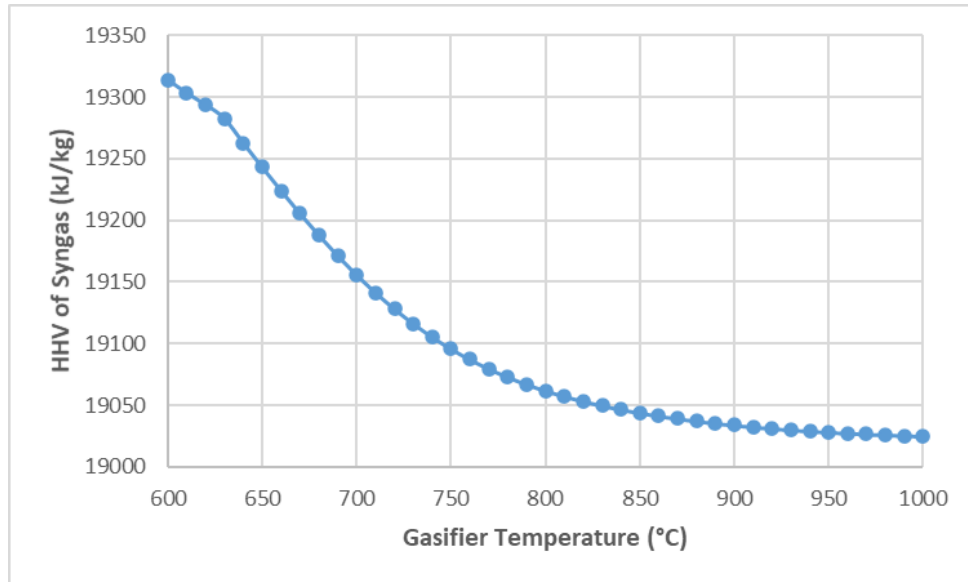


Figure 3. Effect of the temperature on HHV of syngas

The change in HHV of syngas corresponding to increased gasification temperature showed a decreasing tendency, as seen in Figure 3. The calorific value of each component is different; therefore, syngas composition directly affects the HHV of syngas. The decline slowed after 800 °C, this showed similar behavior with the change of CH₄ contents in syngas. Compared to H₂ and CO, CH₄ is three times more effective in terms of energy content and its decreasing content in syngas with enhancement of the gasification temperature caused the drastic reduction in HHV of syngas [45, 46].

3.2.3. Investigation of S/B ratio on Syngas Composition

The S/B ratio is the most influential parameter for steam promoted gasification processes and is determined as the feed rate of the steam divided by the biomass mass flow rate. Steam gasification is preferred due to its advantage of enriching the fraction of H₂ in syngas. The effect of S/B ratio on syngas composition was observed when the gasification temperature fixed at 800 °C in Figure 4.

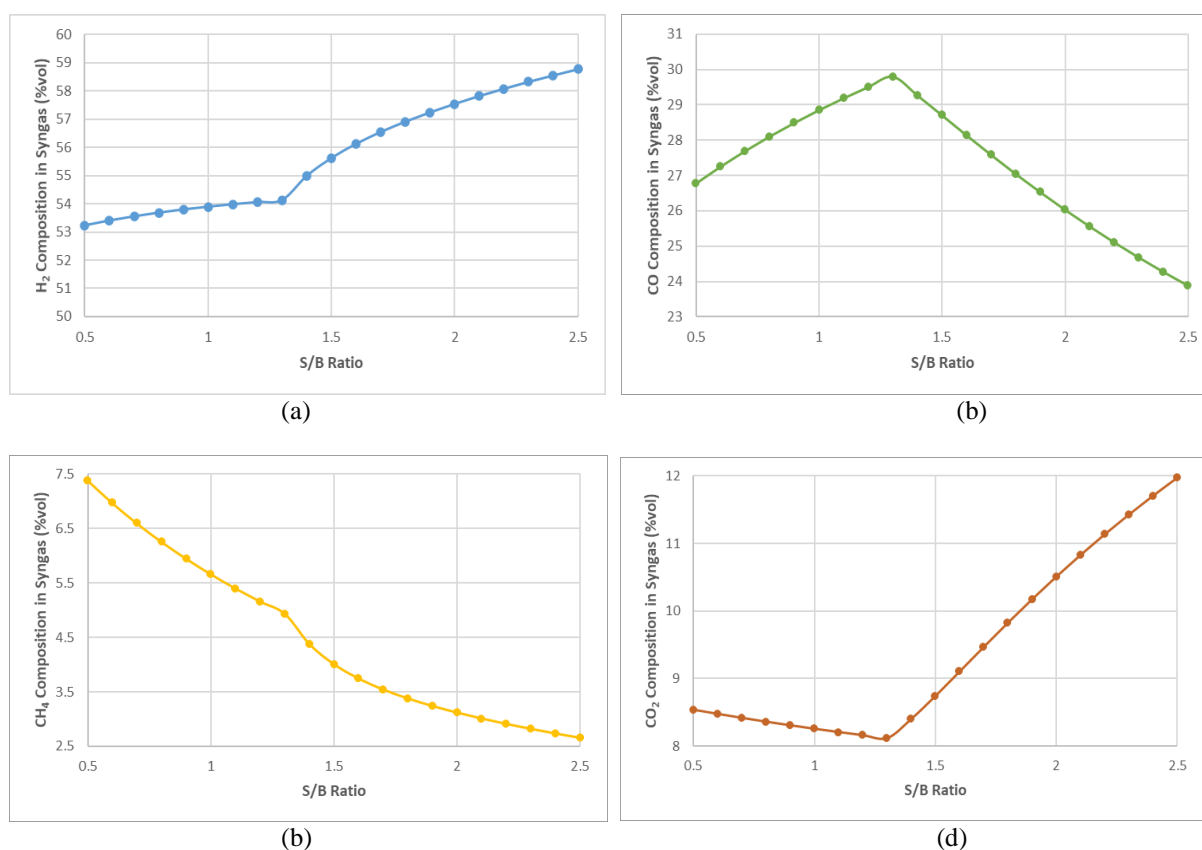


Figure 4. Effect of the S/B ratio on syngas composition (a) H₂, (b) CO, (c) CH₄, (d) CO₂

As seen in Figure 4, syngas composition remarkably changed as a function of the S/B ratio. Increasing the S/B ratio between 0.5 and 2.5 increased the H₂ content in syngas from 53.22% to 58.77% owing to an increase in the partial pressure of steam which encourages the steam methane reforming, water-gas, and water-gas shift ($\text{CO} + \text{H}_2\text{O} \leftrightarrow \text{CO}_2 + \text{H}_2$) reactions inside the gasifier [47]. From Figure 4.b and 4.d, CO composition increased and CO₂ composition decreased until the S/B ratio is 1.3, after this point, their behaviors reversed and CO composition decreased while CO₂ composition increased. H₂ composition showed an opposite tendency with the CH₄ composition because the steam methane reforming reaction uses CH₄ to produce H₂. The results depicted that the composition change in syngas was consistent with the literature studies [23, 48-50]. The optimal S/B ratio was determined as 1.5 considering the higher amounts of H₂ and CO compositions and the lower amount of CO₂.

3.2.4. Investigation of S/B ratio on HHV of Syngas

The proportion of H₂, CH₄, CO₂, and CO in syngas significantly influenced the HHV of syngas as the performance indicator of the gasification process. Thus, the HHV of syngas is affected by the S/B ratio in the gasification processes that use steam as the gasifying agent. The HHV of syngas was directly obtained from the property sets, and sensitivity analysis was conducted as a function of the S/B ratio in Aspen Plus[®].

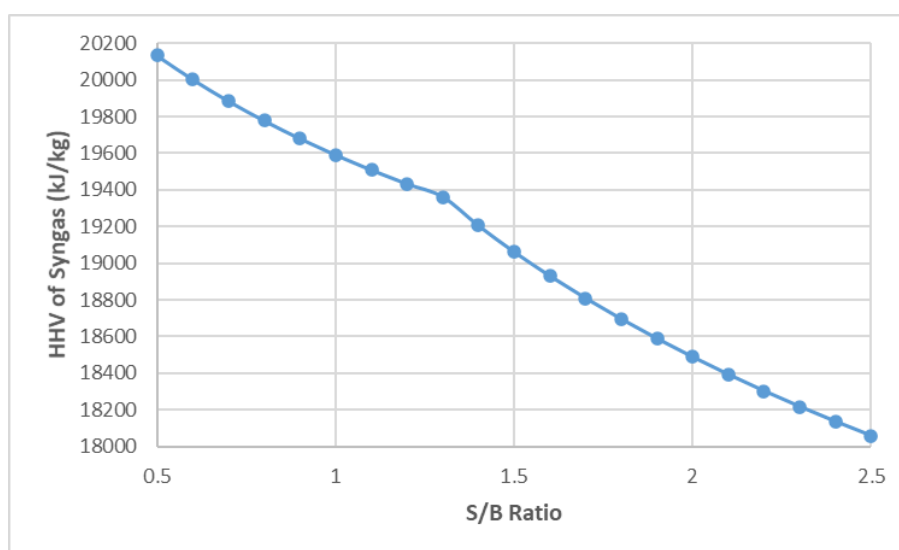


Figure 5. Effect of the S/B ratio on HHV of syngas

The HHV of syngas ratio diminished from 20132 kJ/kg to 18059 kJ/kg while the S/B changed between 0.5 and 2.5, seen in Figure 5. The HHV of syngas sharply dropped, which is similar to CH₄ trend with respect to increasing S/B ratio, because the effect of CH₄ on HHV of syngas is more active than other components as reported in the literature [48, 51]. Considering the syngas composition that desires higher H₂ content and the HHV of syngas, S/B ratio was selected 1.5 as the optimal value.

CONCLUSION

Using the developed downdraft gasifier model, the gasification of the microalgae sample under the steam atmosphere and the production of synthesis gas with high H₂ content were simulated using Aspen Plus[®] software. The compositions of H₂ and CO in the syngas reached their optimal values of 55.62% and 28.70%, respectively, when the operating conditions were a gasification temperature of 800 °C and S/B ratio of 1.5. With the increase of gasification temperature and S/B ratio, the H₂ composition increased appropriately from 50.72% to 56.47% with the increase of gasification temperature and from 53.22% to 58.77% with the increase of S/B ratio. In addition to the syngas composition, the HHV of the syngas was also investigated and showed a decreasing trend with the increase of gasification temperature and S/B ratio due to the CH₄ components, which mainly affect the syngas quality. The presented results of the simulation model, which are in agreement with the literature study, prove that the downdraft gasifier model was properly designed for microalgae gasification.

CONFLICT OF INTEREST

The authors stated that there are no conflicts of interest regarding the publication of this article.

REFERENCES

- [1] Nurcahyani PR, Hashimoto S, Matsumura Y. Supercritical water gasification of microalgae with and without oil extraction. *The Journal of Supercritical Fluids*, 2020;165:104936.
- [2] Mian MM, Zeng X, Nasry AaNB, Al-Hamadani SM. Municipal solid waste management in China: a comparative analysis. *Journal of Material Cycles and Waste Management*, 2017;19:1127-35.

- [3] Heinimö J, Junginger M. Production and trading of biomass for energy—an overview of the global status. *Biomass and Bioenergy*, 2009;33:1310-20.
- [4] Ritchie H, Reay DS, Higgins P. The impact of global dietary guidelines on climate change. *Global Environmental Change*, 2018;49:46-55.
- [5] Cho S, Woo Y-b, Kim BS, Kim J. Optimization-based planning of a biomass to hydrogen (B2H2) system using dedicated energy crops and waste biomass. *Biomass and Bioenergy*, 2016;87:144-55.
- [6] Chen W-H, Lin B-J, Huang M-Y, Chang J-S. Thermochemical conversion of microalgal biomass into biofuels: a review. *Bioresource technology*, 2015;184:314-27.
- [7] Ward A, Lewis D, Green F. Anaerobic digestion of algae biomass: a review. *Algal Research*, 2014;5:204-14.
- [8] Azadi P, Brownbridge GP, Mosbach S, Inderwildi OR, Kraft M. Production of biorenewable hydrogen and syngas via algae gasification: a sensitivity analysis. *Energy Procedia*, 2014;61:2767-70.
- [9] Shin YS, Choi HI, Choi JW, Lee JS, Sung YJ, Sim SJ. Multilateral approach on enhancing economic viability of lipid production from microalgae: a review. *Bioresource technology*, 2018;258:335-44.
- [10] Fang P, Gong Z, Wang Z, Wang Z, Meng F. Study on combustion and emission characteristics of microalgae and its extraction residue with TG-MS. *Renewable Energy*, 2019;140:884-94.
- [11] Duan P, Savage PE. Upgrading of crude algal bio-oil in supercritical water. *Bioresource Technology*, 2011;102:1899-906.
- [12] Raheem A, Cui X, Mangi FH, Memon AA, Ji G, Cheng B, et al. Hydrogen-rich energy recovery from microalgae (lipid-extracted) via steam catalytic gasification. *Algal Research*, 2020;52:102102.
- [13] Zhu Y, Piotrowska P, van Eyk PJ, Boström D, Wu X, Boman C, et al. Fluidized bed co-gasification of algae and wood pellets: gas yields and bed agglomeration analysis. *Energy & Fuels*, 2016;30:1800-9.
- [14] Duman G, Uddin MA, Yanik J. Hydrogen production from algal biomass via steam gasification. *Bioresource Technology*, 2014;166:24-30.
- [15] Panwar N, Kothari R, Tyagi V. Thermo chemical conversion of biomass—Eco friendly energy routes. *Renewable and Sustainable Energy Reviews*, 2012;16:1801-16.
- [16] Adeyemi I, Janajreh I. Modeling of the entrained flow gasification: Kinetics-based ASPEN Plus model. *Renewable Energy*, 2015;82:77-84.
- [17] Nipattummakul N, Ahmed I, Kerdsuwan S, Gupta AK. High temperature steam gasification of wastewater sludge. *Applied Energy*, 2010;87:3729-34.

- [18] Jarunghammachote S, Dutta A. Experimental investigation of a multi - stage air - steam gasification process for hydrogen enriched gas production. *International journal of energy research*, 2012;36:335-45.
- [19] Sansaniwal S, Pal K, Rosen M, Tyagi S. Recent advances in the development of biomass gasification technology: A comprehensive review. *Renewable and Sustainable Energy Reviews*, 2017;72:363-84.
- [20] Xiang X, Gong G, Wang C, Cai N, Zhou X, Li Y. Exergy analysis of updraft and downdraft fixed bed gasification of village-level solid waste. *International Journal of Hydrogen Energy*, 2020.
- [21] Prasertcharoensuk P, Hernandez DA, Bull SJ, Phan AN. Optimisation of a throat downdraft gasifier for hydrogen production. *Biomass and Bioenergy*, 2018;116:216-26.
- [22] Susastriawan A, Saptoadi H. Effect of tuyer distance above grate on propagation front and performance of downdraft gasifier with the feedstock of rice husk. *Renewable Energy*, 2019;134:1034-41.
- [23] Tavares R, Monteiro E, Tabet F, Rouboa A. Numerical investigation of optimum operating conditions for syngas and hydrogen production from biomass gasification using Aspen Plus. *Renewable Energy*, 2020;146:1309-14.
- [24] AlNouss A, Parthasarathy P, Shahbaz M, Al-Ansari T, Mackey H, McKay G. Techno-economic and sensitivity analysis of coconut coir pith-biomass gasification using ASPEN PLUS. *Applied Energy*, 2020;261:114350.
- [25] Kaushal P, Tyagi R. Advanced simulation of biomass gasification in a fluidized bed reactor using ASPEN PLUS. *Renewable Energy*, 2017;101:629-36.
- [26] Nikoo MB, Mahinpey N. Simulation of biomass gasification in fluidized bed reactor using ASPEN PLUS. *Biomass and Bioenergy*, 2008;32:1245-54.
- [27] Adnan MA, Hossain MM. Gasification performance of various microalgae biomass—A thermodynamic study by considering tar formation using Aspen plus. *Energy Conversion and Management*, 2018;165:783-93.
- [28] Adnan MA, Xiong Q, Muraza O, Hossain MM. Gasification of wet microalgae to produce H₂-rich syngas and electricity: a thermodynamic study considering exergy analysis. *Renewable Energy*, 2020;147:2195-205.
- [29] Phyllis2. ECN laboratories.
- [30] Soares RB, Martins MF, Gonçalves RF. A conceptual scenario for the use of microalgae biomass for microgeneration in wastewater treatment plants. *Journal of Environmental Management*, 2019;252:109639.
- [31] Bassyouni M, ul Hasan SW, Abdel-Aziz M, Abdel-hamid S-S, Naveed S, Hussain A, et al. Date palm waste gasification in downdraft gasifier and simulation using ASPEN HYSYS. *Energy Conversion and Management*, 2014;88:693-9.

- [32] Han J, Liang Y, Hu J, Qin L, Street J, Lu Y, et al. Modeling downdraft biomass gasification process by restricting chemical reaction equilibrium with Aspen Plus. *Energy Conversion and Management*, 2017;153:641-8.
- [33] Sezer S, Kartal F, Özveren U. Prediction of chemical exergy of syngas from downdraft gasifier by means of machine learning. *Thermal Science and Engineering Progress*, 2021;26:101031.
- [34] Aspen Technology I. *Getting Started Modeling Processes with Solids*. USA2013.
- [35] Ramos A, Monteiro E, Rouboa A. Numerical approaches and comprehensive models for gasification process: A review. *Renewable and Sustainable Energy Reviews*, 2019;110:188-206.
- [36] Dhanavath KN, Shah K, Bhargava SK, Bankupalli S, Parthasarathy R. Oxygen–steam gasification of karanja press seed cake: Fixed bed experiments, ASPEN Plus process model development and benchmarking with saw dust, rice husk and sunflower husk. *Journal of Environmental Chemical Engineering*, 2018;6:3061-9.
- [37] Ramzan N, Ashraf A, Naveed S, Malik A. Simulation of hybrid biomass gasification using Aspen plus: A comparative performance analysis for food, municipal solid and poultry waste. *Biomass and Bioenergy*. 2011;35:3962-9.
- [38] Sezer S, Özveren U. Investigation of syngas exergy value and hydrogen concentration in syngas from biomass gasification in a bubbling fluidized bed gasifier by using machine learning. *International Journal of Hydrogen Energy*, 2021;46:20377-96.
- [39] Kartal F, Özveren U. A deep learning approach for prediction of syngas lower heating value from CFB gasifier in Aspen plus®. *Energy*, 2020;209:118457.
- [40] Son Y-I, Yoon SJ, Kim YK, Lee J-G. Gasification and power generation characteristics of woody biomass utilizing a downdraft gasifier. *Biomass and Bioenergy*, 2011;35:4215-20.
- [41] Rudra S, Tesfagaber YK. Future district heating plant integrated with municipal solid waste (MSW) gasification for hydrogen production. *Energy*, 2019;180:881-92.
- [42] Sezer S, Kartal F, Özveren U. Artificial Intelligence Approach in Gasification Integrated Solid Oxide Fuel Cell Cycle. *Fuel*, 2022;311:122591.
- [43] Vargas-Moreno J, Callejón-Ferre A, Pérez-Alonso J, Velázquez-Martí B. A review of the mathematical models for predicting the heating value of biomass materials. *Renewable and Sustainable Energy Reviews*, 2012;16:3065-83.
- [44] Shahbaz M, Al-Ansari T, Inayat M, Sulaiman SA, Parthasarathy P, McKay G. A critical review on the influence of process parameters in catalytic co-gasification: Current performance and challenges for a future prospectus. *Renewable and Sustainable Energy Reviews*. 2020;134:110382.
- [45] Kaewluan S, Pipatmanomai S. Potential of synthesis gas production from rubber wood chip gasification in a bubbling fluidised bed gasifier. *Energy Conversion and Management*, 2011;52:75-84.

- [46] Sikarwar VS, Ji G, Zhao M, Wang Y. Equilibrium modeling of sorption-enhanced cogasification of sewage sludge and wood for hydrogen-rich gas production with in situ carbon dioxide capture. *Industrial & Engineering Chemistry Research*, 2017;56:5993-6001.
- [47] Monteiro E, Ismail TM, Ramos A, Abd El-Salam M, Brito P, Rouboa A. Assessment of the miscanthus gasification in a semi-industrial gasifier using a CFD model. *Applied Thermal Engineering*, 2017;123:448-57.
- [48] Mazumder J, de Lasa HI. Catalytic steam gasification of biomass surrogates: Thermodynamics and effect of operating conditions. *Chemical Engineering Journal*, 2016;293:232-42.
- [49] Couto N, Monteiro E, Silva V, Rouboa A. Hydrogen-rich gas from gasification of Portuguese municipal solid wastes. *International Journal of Hydrogen Energy*, 2016;41:10619-30.
- [50] Kartal F, Özveren U. A comparative study for biomass gasification in bubbling bed gasifier using Aspen HYSYS. *Bioresource Technology Reports*, 2021;13:100615.
- [51] Ammar M, Mutalib MA, Yusup S, Inayat A, Shahbaz M, Ali B. Influence of effective parameters on product gas ratios in sorption enhanced gasification. *Procedia Engineering*, 2016;148:735-41.



RESEARCH ARTICLE

THE DETECTION OF EGG SHELL CRACKS USING DIFFERENT CLASSIFIERS

Mehmet YUMURTACI¹ , Zekeriya BALCI^{2,*} , Semih ERGİN³ , İsmail YABANOVA⁴ 

¹ Department of Electrical & Electronics Engineering, Afyon Kocatepe University, Afyon, Turkey

² Department of Electronics and Automation, Van Yüzüncü Yıl University, Van, Turkey

³ Department of Electrical & Electronics Engineering, Eskişehir Osmangazi University, Eskişehir, Turkey

⁴ Department of Electrical Engineering, Manisa Celal Bayar University, Manisa, Turkey

ABSTRACT

Chicken eggs, which are widely consumed in daily life due to their rich nutritional values, are also used in many products. The increasing need for eggs must be met quickly for various circumstances. Eggs are subjected to various impacts and shaken from production to packaging. In some cases, these effects cause an eggshell to crack. While these cracks are sometimes visible, they are sometimes micro-sized and cannot be seen. The cracks on the egg allow harmful micro-organisms to spoil the egg in a short time. In this study, acoustic signals generated by a mechanical effect to the eggs were recorded for 0.2 seconds at 50 kHz sampling frequency using a microphone. To determine the active part in the collected acoustic signal data, a clipping process was implemented by a thresholding process. Thus, the exactly correct moment of mechanical contact on the eggshell was easily detected. After passing the determined threshold value, statistical parameters such as min, max, difference, mean, standard deviation, skewness and kurtosis were extracted from the data obtained, and 7-dimensional feature vectors were created. Finally, the Common Vector Approach (CVA) is applied on the extracted feature vectors, 100% success rate has been achieved for the test data set. The ANN and SVM classifiers in where the same feature vectors are treated were used for the comparison purpose, and exactly the same classification rates are attained; however, the less number of eggs are tested with the ANN and SVM classifiers in the same amount of time. With the proposed mechanical system and classification methodology, it takes about 0.2008 seconds to determine whether the shells of eggs are cracked/intact. Therefore, the proposed combination of the feature vectors based on statistical features and CVA as a classifier for the detection of cracks on eggshells is notably appropriate especially for industrial applications in terms of speed and accuracy aspects.

Keywords: Egg, Eggshell, Common Vector Approach, CompactRIO

1. INTRODUCTION

Egg has become a widely consumed food in the daily diet of people due to its low price and rich nutritional value. Cracks may occur in eggshells during the production or shipping processes. This problem can be resulted in substantial economic losses for egg industry because several harmful bacteria may get into the egg through the cracked shell. An infected egg can also pose an important problem in terms of food safety and human health [1-4]. Detecting and separating the cracks on eggshells are important both for commercial and human health considering the above-mentioned issues.

Egg cracks were attempted to be detected using images taken with the aid of a camera [5]. Several image processing and pattern recognition methods have been applied to eggs under a condition of illuminating light source [5-14]. As a result of these studies, it was observed that the cracks on eggshells were detected with a success rate of more than 90% using several computer vision methods. However, it was reported that both the structural defects on eggshells and the incorrect adjustment of illuminating light source cause a problem in detecting cracks by computer vision methods [15]. These methods are also unable to determine micro cracks. It was reported that 100% success rate can be achieved as a result of the clarification of the cracked area by applying negative pressure to egg for the detection of micro

*Corresponding Author: balcizekeriya29@gmail.com

Received: 02.07.2021 Published: 28.06.2022

cracks with computer vision [16-19]. However, these methods are not suitable for applicability to industry because of both the complexity and slowness issues.

Another method employed in the literature for the detection of eggshell cracks is acoustic signal analysis [20]. This method consists of performing a mechanical contact on eggshells, collecting the acoustic signals resulting from mechanical contact, applying various signal processing and feature extraction methods, and finally, classification. The studies performed in [20-29] reported that the detection of cracks on eggshells was succeeded with at most 98.9% accuracy with acoustic signal analysis and proposed classification methods.

In this paper, the acoustic signal generated by a non-destructive mechanical contact on eggshells was recorded for 0.2 seconds durations with the help of a microphone at a sampling frequency of 50 kHz. In clipping of the active part in the recorded acoustic signal, a 0.75V threshold value was preferred. Thus, the precise accurate moment of mechanical contact on a shell can be easily detected. Statistical features were used to reduce the size of the data signals and to determine the effective parameters from the thresholded data signals. By evaluating the min, max, difference, mean, standard deviation, skewness, and kurtosis values obtained from thresholded acoustic signals, 7-dimensional feature vectors were extracted. Finally, different classifiers are applied to the feature vectors to determine whether an eggshell is cracked or intact.

2. MATERIALS and METHODS

2.1. Experimental Setup

The block diagram of the experimental setup consisting of power supply, control and amplifier circuit, CompactRIO (cRIO), egg support, and mechanical unit for data collection, analysis, and visualization is given in Figure 1. The components are described in detail in the following sections.

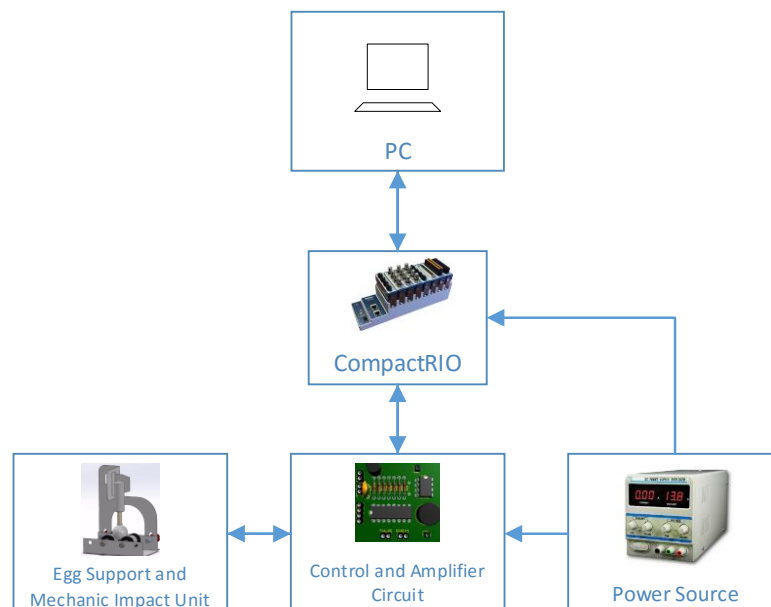


Figure 1. General block diagram of the experimental setup.

2.1.1. CompactRIO

CompactRIO (cRIO) is an application-oriented industrial controller with modular units manufactured by National Instruments (NI) [30]. In this paper, the NI-9215 analog input module and NI-9375 digital input-output module were used together with cRIO 9074. Technical data of cRIO are given in Table 1.

Table 1. Technical data for CompactRIO

Operation Voltage	+19V DC to 30V DC
Processor Speed	400 MHz
Memory	256 MB
FPGA	Xilinx Spartan-3 2M FPGA
Communication Support	Ethernet and RS232
Number of Modular Units	8 Unit

2.1.2. Egg support and mechanical impact unit

Figure 2 shows the general view of setup for the egg support and mechanical impact unit. The egg support unit is the unit on which the egg to be tested is positioned. The mechanical impact unit applies the mechanical impact to the egg and receives the acoustic signal.

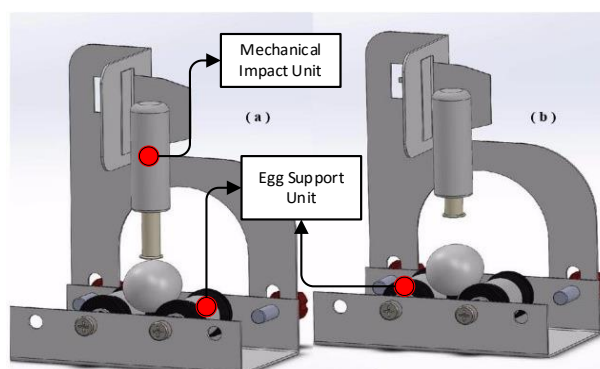


Figure 2. General view of the egg support unit and the mechanical impact unit; (a) the hitting position of the unit to an egg, (b) the starting position of the unit.

The mechanical impact unit consists of a cylindrical outer part on which a coil is wound and a movable cylindrical inner part with a small magnet inside. The movement of the inner part is provided by changing the voltage polarity of the coil wound on the outer part. With this movement, acoustic signals were created as a result of a mechanical impact that is sufficient to generate a mechanical vibration on the egg and does not damage the eggshell. This process is illustrated in Figure 2.

2.1.3. Control and amplifier circuit

The electronic board is designed using L293D and LN358N ICs. With the L293D IC, the mechanical impact unit is driven and the LN358N IC is used to amplify the acoustic signal resulting from the mechanical impact. Electronic card layout is given in Figure 3.

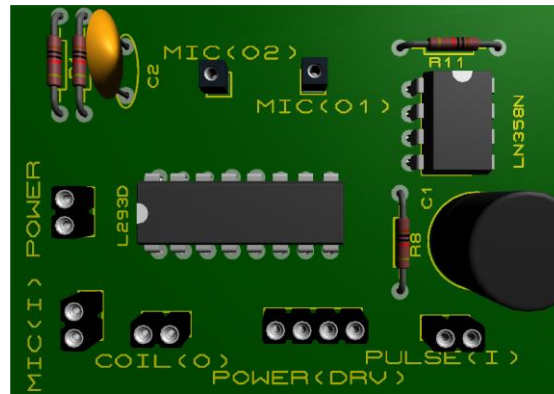


Figure 3. Control and amplifier circuit

2.1.4. Data acquisition program

To create the data set, a data acquisition program was created using the LABVIEW [31] functional blocks, and its screenshot is given in Figure 4. The user interface of the program given in Figure 4, starting with pressing the “get data” button and ends with the acquisition of acoustic data resulting from the mechanical impact applied to the egg, based on the specified sampling time.



Figure 4. Data acquisition program

2.2. Creating the Feature Vector

There are some noises in the raw signals received for 0.2 seconds at 50 kHz sampling frequency via our data acquisition program. Raw signals exceeding a threshold value of 0.75V, which is determined by trial/error methodology, are gathered to detect the data at the moment of mechanical impact on the eggshell, thereby the noisy part can be discarded. Therefore, data signals which have 680 samples are collected. As a result of the examination of these signals obtained from cracked/intact eggs, it was observed that the signal was stable after approximately this amount of data. Then statistical features were extracted to obtain the feature vectors to be fed to the classifier in order to determine cracked/intact

eggshells. A 1x7 dimensional feature vector was constructed using the minimum value, maximum value, difference, mean, standard deviation, skewness, and kurtosis parameters. The equations for statistical features are given in Table 2 [32].

Table 2. Statistical features and their equations.

Feature	Symbol	Equation
min	F_1	$\min\{X_1, X_2, X_3, \dots, X_n\}, 1 \leq n \leq N$
max	F_2	$\max\{X_1, X_2, X_3, \dots, X_n\}, 1 \leq n \leq N$
Difference	F_3	$F_2 - F_1$
Mean	F_4	$\frac{1}{N} \sum_{n=1}^N X_n$
Standard deviation	F_5	$\sqrt{\frac{1}{N} \sum_{n=1}^N (X_n - F_4)^2}$
Skewness	F_6	$\frac{1}{(N-1)(F_5)^3} \sum_{n=1}^N (X_n - F_4)^3$
Kurtosis	F_7	$\frac{1}{(N-1)(F_5)^4} \sum_{n=1}^N (X_n - F_4)^4$

2.3. Common Vector Approach (CVA)

One of the significant subspace methods used in the 1-dimensional pattern recognition problems is CVA [33-36]. The main goal of CVA is to eliminate the differences in a pattern class and to find a single vector that has the unchanging common properties of that class. The CVA is examined in two different cases according to the relationship between the number of feature vectors in training set of a class and the size of feature vectors. These cases are called as insufficient data and sufficient data cases. In the case of sufficient data used in this study, the number of feature vectors (m) belonging to a class is greater than the feature vector dimension (n) ($m > n$). In this case, the common vector belonging to a pattern class is found using the within-class covariance matrix. Let the column wise feature vectors in the training set of a pattern class are $\mathbf{a}_1, \mathbf{a}_2, \dots, \mathbf{a}_m$, respectively. In the sufficient data case realization of CVA, first of all, the covariance matrix belonging to a pattern class is calculated as follow:

$$\Phi = \sum_{i=1}^m [(\mathbf{a}_i - \mathbf{a}_{ave})(\mathbf{a}_i - \mathbf{a}_{ave})^T] \tag{1}$$

Here, \mathbf{a}_{ave} is the average vector of the feature vectors belonging to a class in the training set of the pattern class and Φ shows the within-class covariance matrix belonging to that pattern class.

The eigenvalue-eigenvector decomposition of the within-class covariance matrix is performed, and then, n eigenvalues greater than zero value are obtained. These eigenvalues are sorted in descending order.

The largest k eigenvalues among the eigenvalues are chosen with the help of the following inequality [37]:

$$\frac{\left(\sum_{j=k+1}^n \lambda_j \right)}{\left(\sum_{j=1}^n \lambda_j \right)} \leq Y \quad (2)$$

Where k is the number of largest eigenvalues chosen; λ_j is the eigenvalues, and Y is the fixed percentage value to be used in the eigenvalue selection. If $Y = 5.58\%$, a good performance is obtained while retaining a small proportion of the variance present in the original space. $Y = 5.58\%$ is the average rate for eigenvalues of within-class covariance matrices calculated in each cross-validation step. The value of k was equal to four for each class (intact or cracked egg), and it can also be specified from the point where the eigenvalues of the training data start for varying slowly upon plotting of the eigenvalues in descending order. k eigenvectors corresponding to k eigenvalues of the computed within-class covariance matrix span the difference subspace of that pattern class. The remaining $(n - k)$ eigenvectors will span the indifference subspace of that pattern class. In this circumstance, the projection ($\mathbf{a}_{i,dif}$) of any \mathbf{a}_i feature vector belonging to a pattern class into the difference subspace of that pattern class is calculated as follow [38]:

$$\mathbf{a}_{i,dif} = \sum_{j=1}^k \left[(\mathbf{a}_i^T \mathbf{u}_j) \mathbf{u}_j \right] \quad (3)$$

Here, \mathbf{u}_j are the eigenvectors spanning the difference subspace of that pattern class. The common vector belonging to that pattern class is calculated with the help of the mean vector as follows:

$$\mathbf{a}_{com} = \sum_{j=k+1}^n \left[(\mathbf{a}_{ave}^T \mathbf{u}_j) \mathbf{u}_j \right] \quad (4)$$

After the calculation of the difference/indifference subspaces and the common vector, the training phase of CVA is completed. In the test phase of CVA, the \mathbf{a}_x vector, which will be classified in the pattern test set, is tested using the following decision criteria and assigned to the appropriate class:

$$S^* = \underset{1 \leq C \leq S}{argmin} \left\| \left[\sum_{j=k+1}^n (\mathbf{a}_x - \mathbf{a}_{ave}^C)^T \mathbf{u}_j^C \right] \mathbf{u}_j^C \right\|^2 \quad (5)$$

Where S is the number of classes, \mathbf{u}_j^C are the eigenvectors spanning the indifference subspace of the class C , \mathbf{a}_{ave}^C represents the average vector of the class C , and S^* represents the class to which the unknown \mathbf{a}_x vector was assigned as a result of the testing process.

3. RESULTS and DISCUSSION

A total of 10000 samples of data signal for each egg during 0.2 seconds at 50 kHz sampling frequency were obtained using the system in Figure 2. A data set was created using 60 different eggs with intact shells and 59 different eggs with cracked shells. The raw data signals collected from the eggs with intact and cracked shells are shown in Figure 5. The change of the direction of magnetic field in coil in mechanical impact unit is constituted by the change of the polarity of voltage applied, and thus, the pin

in the coil can move out and in easily. There is also a ball at the end of the pin. Acoustic signals are collected through the microphone installed inside the pin.

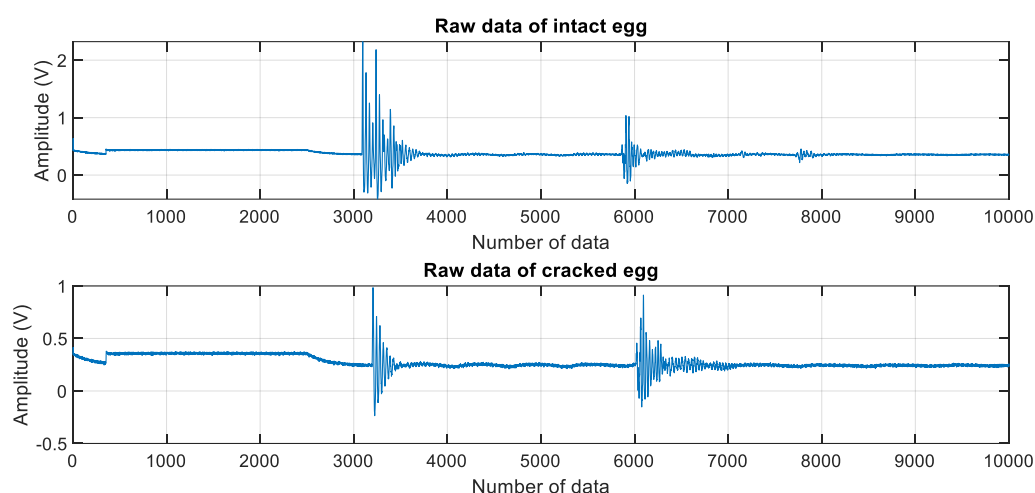


Figure 5. Raw data of eggs with intact and cracked shells

The effect at the moment of contact of the pin on the eggshell and also the effect occurred when it moves back to its starting place are observed in the recorded acoustic signal. A threshold value was determined to obtain useful data from the mechanical impact on the eggshell. In this way, only the acoustic signals generated by the egg were separated from the noisy raw signal generated by the mechanical impact unit and the environment. Starting from the first data point exceeding the 0.75V threshold value from the raw data, 680 data samples were selected. The examples of the selected signal partitions can be seen in Figure 6.

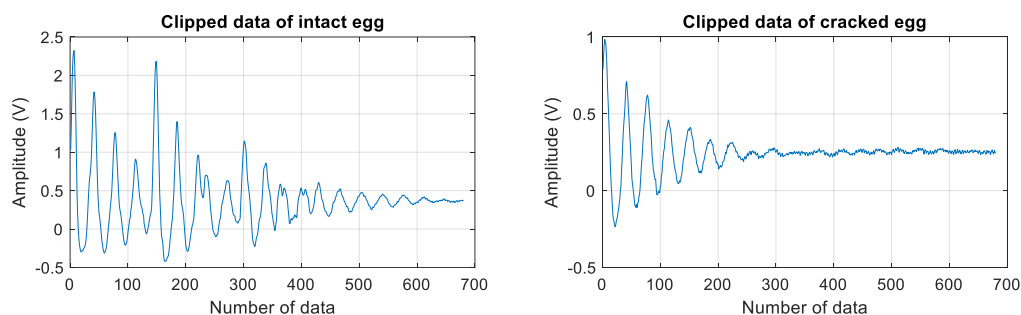


Figure 6. Examples of clipped acoustic signals (each one has 680 samples)

As a result of the mechanical effect, the oscillation of the acoustic signal formed in an intact egg shell is higher than that of in a cracked egg, and the resulting oscillations were damped in a longer time. In the acoustic signal received from an egg with a cracked shell, the oscillation was less and it was damped in a shorter time than an intact egg. The reason for this outcome is that the ball at the end of the pin oscillates more in an egg whose shell is intact.

Feature extraction based on statistical parameters was implemented to feed more effective data to the classifier. Thus, 7-dimensional feature vectors are extracted for each acoustic signal, and then were treated as classifiers. In Table 3, randomly selected feature vectors from the test data of eggs with cracked/intact shells are given.

Table 3. The randomly selected feature vectors of eggs with cracked/intact shells

	Min	Max	Difference	Mean	Standard Deviation	Skewness	Kurtosis
Intact	-0.3619	2.3400	2.7019	0.3862	0.3986	1.5679	7.6146
	-0.2644	2.2696	2.5341	0.4506	0.3574	1.5852	8.1705
	-0.5024	2.8389	3.3413	0.4148	0.5241	1.5083	6.8850
Cracked	-0.1424	1.0062	1.1487	0.3035	0.1165	1.1644	14.5977
	0.0913	0.9922	0.9008	0.4475	0.1016	1.1130	12.1071
	-0.3326	1.0897	1.4223	0.1696	0.1499	1.2530	12.5297

The change in the parameters of maximum, difference, standard deviation, skewness, and kurtosis is seen more effectively among the feature vector parameters obtained by processing an acoustic signal from a cracked/intact egg. The CVA classifier was trained using feature vectors of 10 intact and 10 cracked eggs randomly selected from the data set consisting of 60 eggs with intact shells and 59 eggs with cracked shells (Table 4).

Table 4. Training/test data and performance of the CVA classifier

	Intact	Cracked	Success
Training	10	10	100%
Test	50	49	100%

When the literature studies on the detection of cracked/intact eggshell by processing the acoustic signal resulting from the mechanical effect on an eggshell are examined, there is not an available data set on this subject, and each researcher creates his/her own data set. Ketelaere et al. (2010) applied Fast Fourier Transform (FFT) to the acoustic signal recorded from eggshells at 50 kHz sampling frequency. The Pearson correlation coefficients of the processed acoustic signal were found and the coefficients exceeding over a threshold value are determined; finally, the cracked/intact conditions of shells were determined with a 90% success rate [39]. Deng et al. (2010) applied Continuous Wavelet Transform to the acoustic signal recorded at 22.05 kHz sampling frequency. They achieved a 98.9% success rate by estimating with SVM using different combinations of wavelet-based extracted features [22]. Sun et al. (2013) transferred the data from the time domain recorded with 38 kHz sampling frequency into the frequency domain with FFT. A calibration model was created and five features were extracted from magnitude response of each signal in the frequency domain. If the value of three or more features exceeds their critical values, the eggshell is considered to be intact, otherwise is cracked. While the average performance rate was 98.05%, this method requires less time than 10ms to determine the state of the shell from raw data signal of an egg [40]. In this study, an acoustic signal was collected from an eggshell in 0.2 seconds at 50 kHz sampling frequency. Approximately 0.212 seconds in ANN, 0.205 seconds in SVM, and 0.2008 seconds in CVA are required for processing raw data signals. The consumed time values comprise of the extraction of a feature vector, and performing the estimation process by a classifier. Thus, the shell of 16981 eggs is tested with ANN for an hour. In the same amount of time, additional 579 eggs with SVM and 947 eggs with CVA can be tested. The performance rate for CVA, ANN, and SVM classifiers in where the same feature vectors are treated was determined as 100%. Since the classification process for an egg can be done in totally about 0.2008 seconds, the combination of the feature vectors based on statistical features and CVA as a classifier is considerably suitable for industrial applications.

The 5-fold cross validation technique was performed to evaluate the performance of the feature vector and the CVA classifier. All egg data were randomly divided into five groups; each one includes eggs with 10 cracked shells and 10 intact shells. While one group of data was used in the training phase of the CVA classifier, the remaining four groups of data were used in the testing process. The performance

for each cross-validation step was found to be 100%, therefore, the average testing performance was computed as 100%.

An interface was created with Matlab/GUI to determine the cracked/intact situation in an eggshell collecting/processing/classifying data from the system. By pressing the "Get Data/Analyze" button in Figure 7, the raw data signal taken from an egg is plotted on the graphical display. The raw data signal can be analysed in detail using the tools on the interface. Data is clipped using the threshold value. The feature is extracted and fed to the classifier. At the end of the classification, the decision (either cracked or intact) is printed on the interface and also shown visually on the screen.

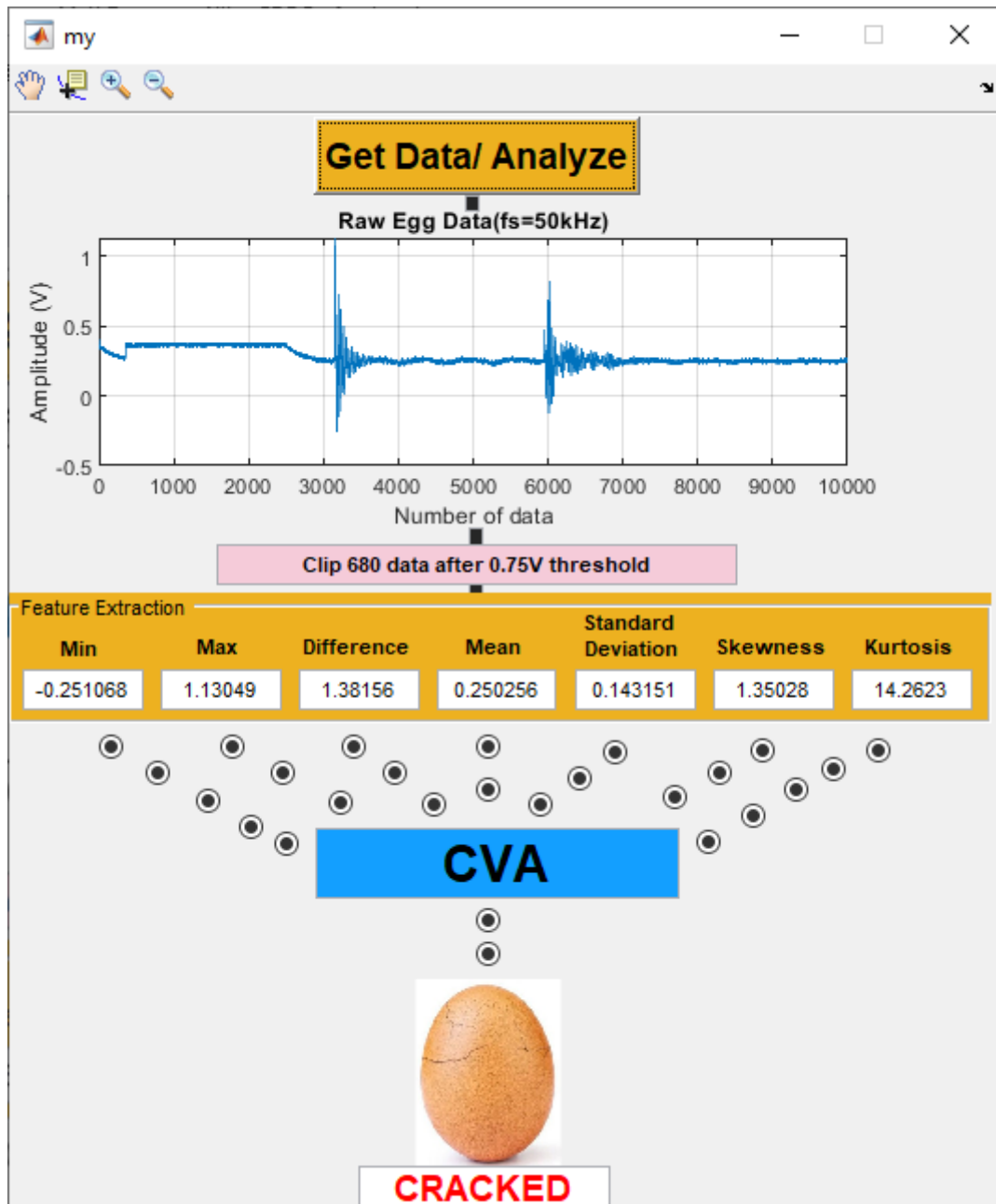


Figure 7. Eggshell control interface

4. CONCLUSION

Chicken eggs are exposed to various impacts and are shaken from the production to the packaging stages and several cracks may occur in their shells. These cracks can be micro-sized and invisible and also cause an egg to deteriorate in a short time. In this study, the acoustic signals generated as a result of the contact made by a mechanical system in a way that it does not damage the eggshell are recorded with a microphone. The active part in acoustic signal was determined by thresholding acoustic signal using a pre-determined value. The statistical features were evaluated, and a feature vector with a size of 1x7 was extracted from each thresholded acoustic signal. For the training of the CVA classifier, 20 data signals, including separately ten feature vectors selected randomly from cracked and intact eggs, were used; and, the other remaining 99 egg data signals in the data set were used in the test process. Although the training process was carried out with a very few data feature vector, all of the test data signals were correctly classified. It takes an average of 0.2008 second for data signal to be retrieved from an egg, pre-processed, and estimated by the CVA classifier. The combination of the extracted feature vector and the CVA classifier are practically suitable for industrial applications due to the speed and accuracy issues for the process of cracked/intact detection of eggshells. Although exactly the same accuracy rates are obtained for CVA, ANN, and SVM classifiers, the less number of eggs are tested with the ANN and SVM classifiers in the same amount of time.

CONFLICT OF INTEREST

The authors stated that there are no conflicts of interest regarding the publication of this article.

REFERENCES

- [1] Singh M, Brar J. Egg safety in the realm of preharvest food safety. *Microbiol. Spectr* 2016; 4(4):o. 4, Aug. 2016, DOI: 10.1128/microbiolspec.PFS-0005-2014.
- [2] Mazzuco H, Bertechini A-G. Critical points on egg production: causes, importance, and incidence of eggshell breakage and defect. *Ciência e Agrotecnologia*, 2013; 38(1): 7–14.
- [3] Van Mourik S, Alders B, Helderma F, van de Ven L-J-F, Koerkamp P-W-G-G. Predicting hairline fractures in eggs of mature hens. *Poult. Sci.*, 2017; 96(6): 1956–1962.
- [4] Widdicombe J-P, Rycroft A-N, Gregory N-G. Hazards with cracked eggs and their relationship to eggshell strength. *J. Sci. Food Agric*, 2009; 89(2): 201–205.
- [5] Wu L, Wang Q, Jie D, Wang S, Zhu Z, Xiong L. Detection of crack eggs by image processing and soft-margin support vector machine *J. Comput. Methods Sci. Eng.*, 2018; (18)1: 21–31.
- [6] Abdullah M-H, Nashat S, Anwar S-A, Abdullah M-Z. A framework for crack detection of fresh poultry eggs at visible radiation. *Comput. Electron. Agric.*, 2017; 141: 81–95.
- [7] Fang W, Youxian W. Detecting preserved eggshell crack using machine vision. In 2011 International Conference of Information Technology, Computer Engineering and Management Sciences, 2011; 3: 62–65.
- [8] Omid M, Soltani M, Dehrouyeh M-H, Mohtasebi S-S, Ahmadi H. An expert egg grading system based on machine vision and artificial intelligence techniques. *J. Food Eng*, 2013; 118(1): 70–77.

- [9] Wang F, Zhang S, Tan Z. Non-destructive crack detection of preserved eggs using a machine vision and multivariate analysis. *Wuhan Univ. J. Nat. Sci.*, 2017; 22(3): 257–262.
- [10] Öztürk N. Görüntü işleme teknikleri ile beyaz yumurtalar üzerindeki yumurta kabuğu kusurlarının algılanması. MSc, Karadeniz Teknik Üniversitesi, Trabzon, Turkey, 2014.
- [11] Abbaspour-gilandeh Y, Azizi A. Identification of cracks in eggs shell using computer vision and hough transform. *Yüzüncü Yıl Üniversitesi Tarım Bilimleri Dergisi*, 2019; 28(4): 375-383.
- [12] Türkoğlu M. Yumurta kabuğu görüntülerinde kırık tespiti için daha hızlı bölgesel tabanlı çok katmanlı evrişimsel sinir ağları. *Gazi University Journal of Science*, 2021; 9(1): 148-157.
- [13] Chen H, Ma J, Zhuang Q, Zhao S, Xie Y. Submillimeter crack detection technology of eggs based on improved light source. In *IOP Conference Series: Earth and Environmental Science*, 22-25 January 2021; Guangzhou, China. 697.
- [14] Dong J, Lu B, He K, Li B, Zhao B, Tang X. Assessment of hatching properties for identifying multiple duck eggs on the hatching tray using machine vision technique. *Computers and Electronics in Agriculture*, 2021; 184:106076.
- [15] Orlova Y, Linker R, Spektor B. Expansion of cracks in chicken eggs exposed to sub-atmospheric pressure. *Biosyst. Eng.*, 2012; 112(4): 278–284.
- [16] Lawrence K-C, Yoon S-C, Jones D-R, Heitschmidt G-W, Park B, Windham W-R. Modified pressure system for imaging egg cracks. *Trans. ASABE*, 2009; 52(3): 983–990.
- [17] Lawrence K-C, Yoon S-C, Heitschmidt G-W, Jones D-R, Park B. Imaging system with modified-pressure chamber for crack detection in-shell eggs. *Sens. Instrum. Food Qual. Saf.*, 2008; 2(2): 116–122.
- [18] Li Y, Dhakal S, Peng Y. A machine vision system for identification of micro-crack in eggshell. *J. Food Eng.*, 2012; 109(1): 127–134.
- [19] Priyadumkol J, Kittichaikarn C, Thainimit S. Crack detection on unwashed eggs using image processing. *J. Food Eng.*, 2017; 209: 76–82.
- [20] Wang H, Mao J, Zhang J, Jiang H, Wang J. Acoustic feature extraction and optimization of crack detection for eggshell. *J. Food Eng.*, 2016; 171: 240–247.
- [21] Lin H, Zhao J, Chen Q, Cai J, Zhou P. Eggshell crack detection based on acoustic response and support vector data description algorithm. *Eur. food Res. Technol.* 2009; 230(1): 95–100.
- [22] Deng X, Wang Q, Chen H, Xie H. Eggshell crack detection using a wavelet-based support vector machine. *Comput. Electron. Agric.* 2010; 70(1): 135–143.
- [23] Zhao Y, Wang J, Lu Q, Jiang R. Pattern recognition of eggshell crack using PCA and LDA. *Innov. Food Sci. Emerg. Technol.* 2010; 11(3): 520–525.
- [24] Ding T, Lu W, Zhang C, Du J, Ding W, Zhao X. Eggshell crack identification based on Welch power spectrum and generalized regression neural network (GRNN). *Food Sci* 2015; 36: 156–160.

- [25] Wang S-C, Ren Y-L, Chen H, Xiong L-R, Wen Y-X. Detection of cracked-shell eggs using acoustic signal and fuzzy recognition. *Transactions CSAE* 2004; 20(4): 130–132.
- [26] Strnková J, Nedomová Š. Eggshell crack detection using dynamic frequency analysis. *MENDELNET*; 2013; Brno. 603-608.
- [27] Jin C, Xie L, Ying Y. Eggshell crack detection based on the time-domain acoustic signal of rolling eggs on a step-plate, *J. Food Eng.*, 2015; 153: 53–62.
- [28] Li P, Wang Q, Zhang Q, Cao S, Liu Y, Zhu T. Non-destructive detection on the egg crack based on wavelet transform. *IERI Procedia*, 2012; 2: 372–382.
- [29] Sun L, Feng S, Chen C, Liu X, Cai J. Identification of eggshell crack for hen egg and duck egg using correlation analysis based on acoustic resonance method. *J. Food Process Eng.*, 2020;13430.
- [30] CompactRIO - Wikipedia. <https://en.wikipedia.org/wiki/CompactRIO>. (accessed Feb. 09, 2020).
- [31] LabVIEW - Vikipedi. <https://tr.wikipedia.org/wiki/LabVIEW> (accessed Feb. 09, 2021).
- [32] Elibol S-G, Yumurtacı M, Ergin S, Yabanova İ. Classification of dynamic EGG weights using feature extraction methods. *Eskişehir Technical University Journal of Science and Technology A - Applied Sciences and Engineering*, 2020; 21(4):499-513.
- [33] Gülmezoğlu M-B, Dzhafarov V, Keskin M, Barkana A. A novel approach to isolated word recognition, *IEEE Trans. on Acoustic Speech and Signal Processing*, 1999; 7(6): 620-628.
- [34] Gülmezoğlu M-B, Dzhafarov V, Barkana A. The common vector approach and its relation to principal component analysis. *IEEE Trans. on Speech and Audio Processing*, 2001; 9(6): 655-662.
- [35] Gülmezoğlu M-B, Dzhafarov V, Edizkan R, Barkana A. The common vector approach and its comparison with other subspace methods in case of sufficient data. *Computer Speech and Language*, 2007; 21: 266-281.
- [36] Gülmezoğlu, M-B, Ergin S. An approach for bearing fault detection in electrical motors, *European Trans. on Electrical Power*, 2007; 17(6): 628-641.
- [37] Oja E. *Subspace methods of pattern recognition*. John Wiley and Sons, Inc.: New York, 1983.
- [38] Gülmezoğlu M-B, Dzhafarov V, Edizkan R, Barkana A. The common vector approach and its comparison with other subspace methods in case of sufficient data, *Computer Speech and Language*, 2007; 21: 266-281.
- [39] De Ketelaere B, Coucke P, De Baerdemaeker J. Eggshell crack detection based on acoustic resonance frequency analysis. *J. Agric. Engng Res.*, 2000; 76: 157-163.
- [40] Sun L, Bi X-k, Lin H, Zhao J-w, Cai J-r. On-line detection of eggshell crack based on acoustic resonance analysis. *Journal of Food Engineering*, 2013; 116: 240-245.



RESEARCH ARTICLE

SOLAR ENERGY ASSISTS SEDIMENT MICROBIAL FUEL CELL TO GENERATE
GREEN ENERGY FROM LIQUID ORGANIC WASTE

Onur Can TÜRKER * 

Aksaray Technical Sciences Vocational School, Department of Environmental Protection, Technologies, Aksaray, Turkey

ABSTRACT

Simultaneous liquid organic waste disposal and electricity generation were achieved by a solar-assist sediment microbial fuel cell (S-SMFC) in terms of an ecological and economical perspective. In this respect, 840 mL house environment liquid organic wastes which contains 10% juice + 90% deionized water and 10% sugary tea + 90% deionized water were disposed by electrogenic bacteria and converted electricity with solar energy. A 100 F capacitor was easily charged 29 times with generated electricity. S-SMFC was disposed 10 mL more waste than control due to more electrical bacteria density on the graphite electrode. In this case, Proteobacteria and Firmicutes were categorized dominate bacteria groups, and they were found in the S-SMFC as 54% and 28%, respectively. Importantly, solar energy increased population density of these groups in the S-SMFC and the density on the graphite electrode increased more than 19% according to control. Some bacteria which were associated with electricity production in the S-SMFC were to *Azospirillum fermentarium*, *Clostridium sp.*, *Pseudomonas guangdongensis*, *Bacteroides sp.*, *Azovibrio restrictus*, *Clostridium pascui*, *Levilinea saccharolytica*, *Seleniivibrio woodruffii*, *Geovibrio ferrireducens*. Consequently, S-SMFC presents innovative, crucial and simple methodology in order to convert liquid organic waste into the green energy.

Keywords: Green energy, Sediment microbial fuel cell, Electrogenic bacteria, Organic waste

1. INTRODUCTION

Uncontrolled liquid organic waste may create potential environmental pollution in the ecosystems when these wastes reach into surface waters [1]. High-polluted organic waste are generally produced house environment (i.e. kitchen), and then join in sewage system or receiving environment after being processed in a central treatment plant [1, 2]. Unfortunately, these type of wastes are directly discharged into receiving environment following the deep sea discharge system without any treatment in recent months due to the inadequacy of the treatment plants [3]. Moreover, the spent time of people at home because of Covid-19 pandemic, the discharge of such waste in the sewage systems increase nowadays. In this respect, some crucial environmental problem (i.e. sea snot or marine mucilage) associated with uncontrolled liquid organic wastes that contain nitrogen and phosphate have often appeared both in world and Turkey [4, 5]. Correspondingly, the marine mucilage has intensively detected in Marmara Sea in Turkey in March-May 2021, and 12,741.94 ha of sea area covered by mucilage [4].

Although this kind of liquid waste can be treated or controlled by conventional techniques (biological treatment, reverse osmosis, ion exchange systems, etc.), these methods requires high chemical use (i.e. barium chloride lime), high energy needs (0.5 kwh for 1 ton of wastewater purification) and expensive equipment (i.e. cationic membranes) [6, 7]. Furthermore, these conventional techniques have only treatment efficiency between 70% and %80 in the purification process[7, 8]. In this respect, new holistic approach and innovation techniques need to on-side control of this type waste prevent from clean water sources or asses this waste for bioenergy sources in terms of secondary benefits [9, 10]. Sediment microbial fuel cell is a simple, cost effective, and environmental friendly method to assess organic substrate (wastewater, rhizosphere excretion) for fuel and generate green energy simultaneously [11,

12]. Briefly, sediment microbial fuel cell is based on the idea of imitating the physical, chemical and biological mechanisms that occur in wetland matrix, and the liquid organic wastes can easily disposal to produce clean energy from organic substrates through electrogenic bacteria without generating any secondary waste [11, 13]. Correspondingly, the liquid organic wastes released into the nature are not considered as waste for sediment microbial fuel cell, this kind of waste are defined as a new energy fuel source to generate green energy in the waste management strategy [9, 14]. In order to eliminate the energy shortage that may occur in the near future, the sediment microbial fuel cell devices provide crucial strategy associated with electrochemical activity comes from catalytic activity of organic substrate, and then electrogenic bacteria can convert organic substrate to green energy [15]. Unfortunately, produced potential green energy by sediment microbial fuel cell is usually low. For example, up to 70% wastewater treatment efficiencies were obtained from constructed wetland couple with sediment microbial fuel cell device, only 198.8 mW/m² power density was produced by the SMFC device [16]. Although this phenomenon is an acceptable level of organic treatment from wastewater, the power density obtained from SMFC significantly limits the usage network of SMFC to generate bioelectricity for real scale application. Furthermore, power generation with organic wastes released from plant roots to the environment in plant sediment microbial fuel cells was recorded as 1 mWatt [17]. In this respect, the obtained low power from SMFC limits use of this type device for practical on-site application for bioelectricity production (i.e. landscape lighting). Consequently, innovative approaches or technological designs are necessary to how to increase power from SMFC while the wastewater treated more efficient and more economical.

In this study, a solar energy assists sediment microbial fuel cell (S-SMFC) was tested to generated bioelectricity from liquid organic waste. Briefly, the purpose of the current study was to: (i) design a solar assist sediment microbial fuel cell to generate bioelectricity from liquid organic waste; (ii) investigate electricity production by electrogenic bacteria and solar energy in the same systems at the first time in the literature; (iii) discuss electricity production mechanism of this hybrid system and compare produced green energy from control.

2. MATERIAL AND METHODS

2.1. Sampling and Bacteria Culture

Sediment sample was collected a wetland habitat (depth of 60cm) in Turkey, and then the sample was mixed with an anaerobic culture that collected from an active sludge reactor. The mixture was transferred into a plastic container inoculated for one month. Nitrogen gas (80%) was applied into the mixture 20 minutes once a day in order to removed oxygen and created anaerobic environment for electrogenic bacteria. Supported culture was prepared, and Proteobacteria composition was enriched in the culture [18]. Accordingly, 15mM sodium acetate was used as carbon sources, 7.1 mM NH₄Cl d for nitrogen sources, and 3mM BES solution for methanogenic inhibitor in the culture. Furthermore, sterilized mineral solution was also added into the culture solution in order to supported to bacterial growth. Correspondingly, 1mL mineral solution is contained per liter: 5.6 g (NH₄)₂SO₄, 2 g MgSO₄·7H₂O, 200 mg MnSO₄·H₂O, 3 mg H₃BO₃, 2.4 mg CoCl₂·6H₂O, 1 mg CuCl₂·2H₂O, 2 mg NiCl₂·6H₂O, 5 mg ZnCl₂, 10 mg FeCl₃·6H₂O, and 0.4 mg Na₂MoO₄·2H₂O).

2.2. Experimental Design

Rectangular polyester containers (13x13 cm) with volume of 500 mL were selected as treatment and control reactor in order to obtained sediment microbial fuel cell (SMFC) environment. Volume of anode chamber in each reactor was 150 mL, and the anode and cathode chamber was separated by glass wool and clay layer (1mm). The anode electrode of each SMFC reactor was a horizontal rectangular graphite plate (100 mm X 100 mm and 60 mm thickness), and cathode electrodes were graphite felt with a diameter of 130 mm. Zeolite mineral was selected as supporting media, and the anode chamber of the

reactors was filled with this material. Graphite electrode was buried into the mixing and peat sample with contains 3% NaCl was added on the separator (glass wool and clay layer) and creating a salt bridge in each reactor matrixes. The cathode electrodes for each reactor were placed on the peat, and they were connected by anodes with high anti-corrosion and good electrical conductivity of 0.8 mm titanium wire. The external resistance was selected as 25Ω in order to obtain a current and increase population of electrogenic bacteria in the reactor matrix. The designed SMFC reactors both treatment and control was cultivated for one month in thermostatically controlled chamber at $35.8 \text{ }^\circ\text{C}$. After cultivation period, 2V 20 mA solar panel was connected in parallel with treatment reactor, and this hybrid system was powered by sediment microbial fuel cell and solar energy, and so the hybrid system was named as S-SMFC (Figure 1). Conversely, the control reactor was only powered by sediment microbial cell that namely as C-SMFC. The reactors were located at the window that directly meet sunlight, and the average temperature was measured as 25°C . An acid-based catalyzer was added into cathode chamber in order to increase open circuit voltage of the reactor.

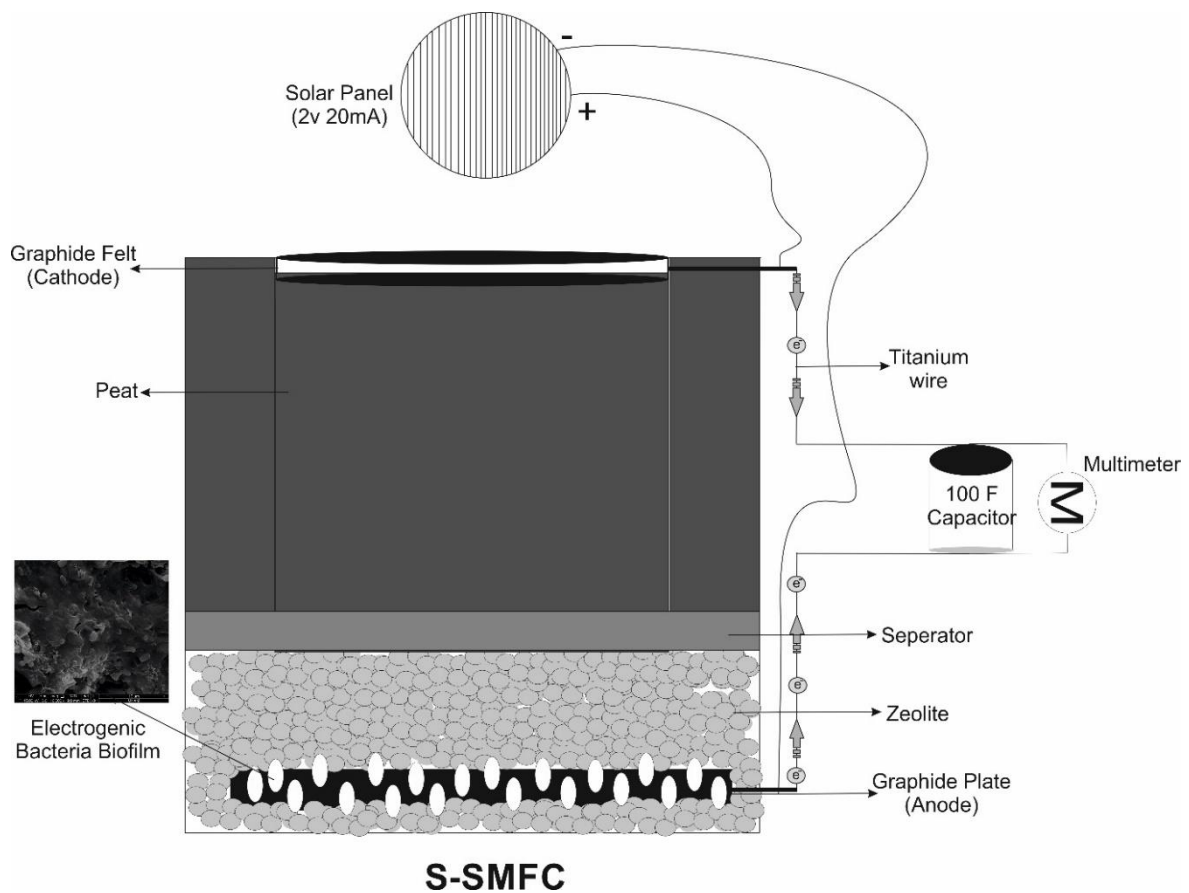


Figure 1. Schematic demonstration of Solar assist sediment microbial fuel cell (S-SMFC)

2.3. Waste Dosage, Measurement, and Analysis

A wide spread liquid organic waste (10% juice waste + 90% deionized water or 10% sugary tea waste + 90% deionized water) produced in household environment was selected for waste in this experiment, and 15 ml waste was added into each reactor in a day. In this case, approximately 110 mL liquid waste was assessed and controlled on the side by reactors in one week, and the waste was converted to electricity by electrogenic bacteria in the SMFC reactors. Produced electricity from each reactor was recorded daily by a multimeter, and then stored 100 F capacitor. After 60 days of operation, the graphite anodes were collected from the reactors and a field-emission scanning microscope was used to determine the biofilm settled on the graphite electrodes. Furthermore, anodic biofilm on the electrodes were

separately collected from both S-SMFC and C-SMFC, and metagenomics analysis was evaluated. The temperature of experiment condition was continually measured by a digital thermometer. Furthermore, the charged capacitor from the reactors were serially connected each treatment day, and the Ni-Cd based battery (1.2 V 800 mAh) was charged these capacitors.

3. RESULTS AND DISCUSSIONS

3.1. Voltage Output and Electricity Generation Assessment

The electricity production performance of the reactors both S-SMFC and C-SMFC were shown in Figure 2a. Correspondingly, the S-SMFC was generated open circuit potential between 1542 and 1919 mV for 10% juice waste, and between 1442 and 1978 mV for 10% sugary Tea waste during the experiment period. This results indicated that the SMFC and solar energy were together produced open circuit potential while the waste broke to pieces, and thus this kind of hybrid system can be used as generated clean energy. On the other hand, the generated electricity from C-SMFC was relatively lower than S-SMFC and output open circuit voltage was ranged from 979 and 1428 mV during the experiment period. Moreover, statistical analysis was also suggested that generated voltage from S-SMFC higher than C-SMFC ($p < 0.05$), and thus it can be concluded that high voltage can be generated for a SMFC when it hybridizing with solar energy. The mentioned from material and method section that solar energy was produced from 2V mini solar panel and it can be emphasized that the panel adequate power and current for assisting density population on the anode surface.

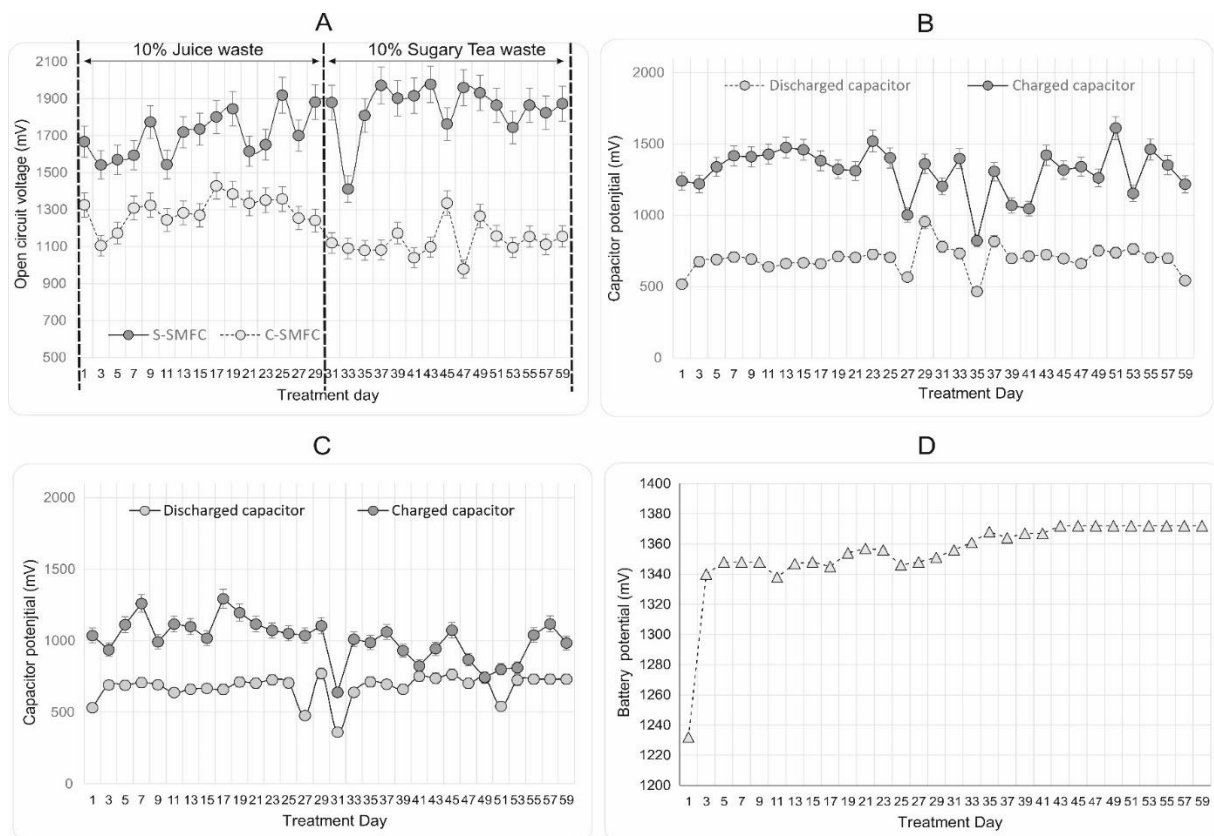


Figure 2. Open circuit voltage of S-SMFC and C-SMFC according to different liquid organic waste (a), Charged and discharged capacitor potential of S-SMFC (b), Charged and discharged capacitor potential of C-SMFC (c), and Battery potential that charged by serially connected capacitors in the experiment period (d).

The generated electricity from reactors were storage in capacitors, and the charged and discharged potential of capacitors were shown in Figure 2b, 2c. In parallel with output voltage in the reactors, the capacitor potential increased with generated electricity from S-SMFC, and the electricity was ranged from 821 to 1621 mV in the experiment period. Furthermore, capacitor potential which connected in C-SMFC also increased with produced electricity, and ranged from 639 to 1294 mV during the treatment days. These results indicated that the reactors produced storing form of electricity from the waste and solar energy, and stored electricity from S-SMFC was higher than C-SMFC. The statistical analysis suggested that capacitor potential for S-SMFC significantly higher than capacitor for C-SMFC ($p < 0.05$). The battery potential result was also confirmed that the reactors generated to storing form of electricity during the experiment period, and thus the potential was increased from 1232 to 1372 mV in the experiment period (Figure 2d).

3.2. Waste Disposal Analysis

The average waste (10% juice waste and 10% sugary tea waste) disposal both in S-SMFC and C-SMFC during the experiment period are shown in Figure 3a. Correspondingly, 840 mL liquid organic waste was used as fuel to generate electricity in S-SMFC, whereas C-SMFC was used 830 mL liquid organic waste in order to produced bioelectricity in the same operational condition during the experiment period. These results indicated that organic compounds in the S-SMFC converted faster to electricity by microbial metabolism compare to C-SMFC. Thus, it can be hypothesized that solar energy increased current in the S-SMFC matrix, and more current led to increasing bacterial density in the graphite electrode. In this case, the increasing bacterial density in the electrode of S-SMFC converted more waste to bioelectricity compare to electrode of C-SMFC in the experiment period. The SEM images from the graphite electrodes were confirmed to this phenomenon that high bacterial density can be seen on the graphite electrode that obtained by S-SMFC (Figure 4a). Similar evidences were also reported by various researchers who indicated that increased current on the graphite led to increasing bacterial population on the electrodes. Accordingly, Kim et al. [19] was found that the bioelectricity current increased when the external resistance (below 100 Ω) connected by parallel in a MFC. Same researcher was reported that high current flow on the graphite electrode due to high external resistance increased electrogenic bacteria population. On the other hand, Commoult et al. [18] also reported that high current flow and low anodic potential (-400 mV) on the electrode increased electrogenic bacteria population in the culture.

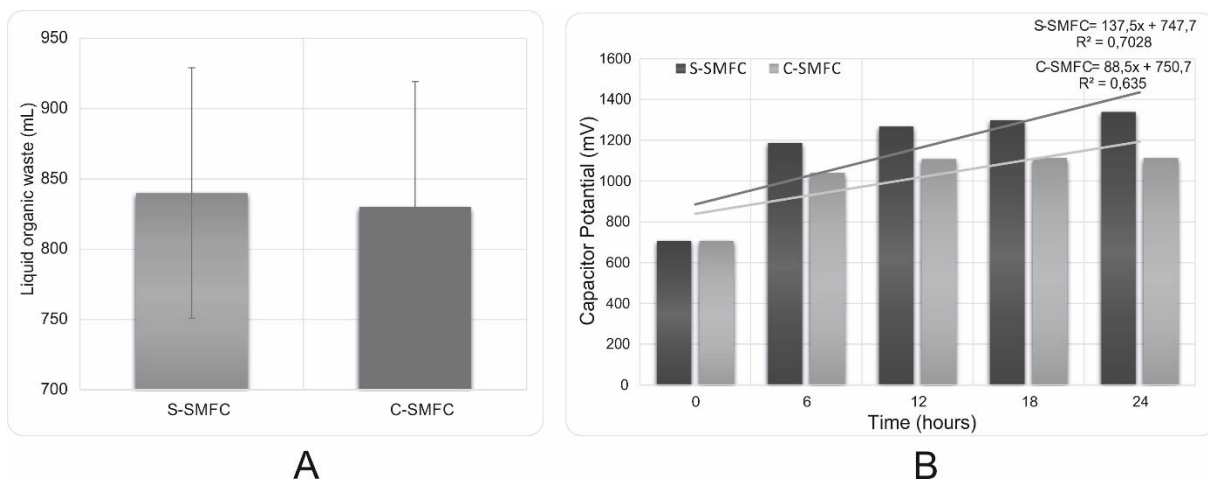


Figure 3. Disposal liquid organic waste volume in S-SMFC and C-SMFC in the experiment period (A), and Charged kinetics of capacitor from the reactors according to time (B).

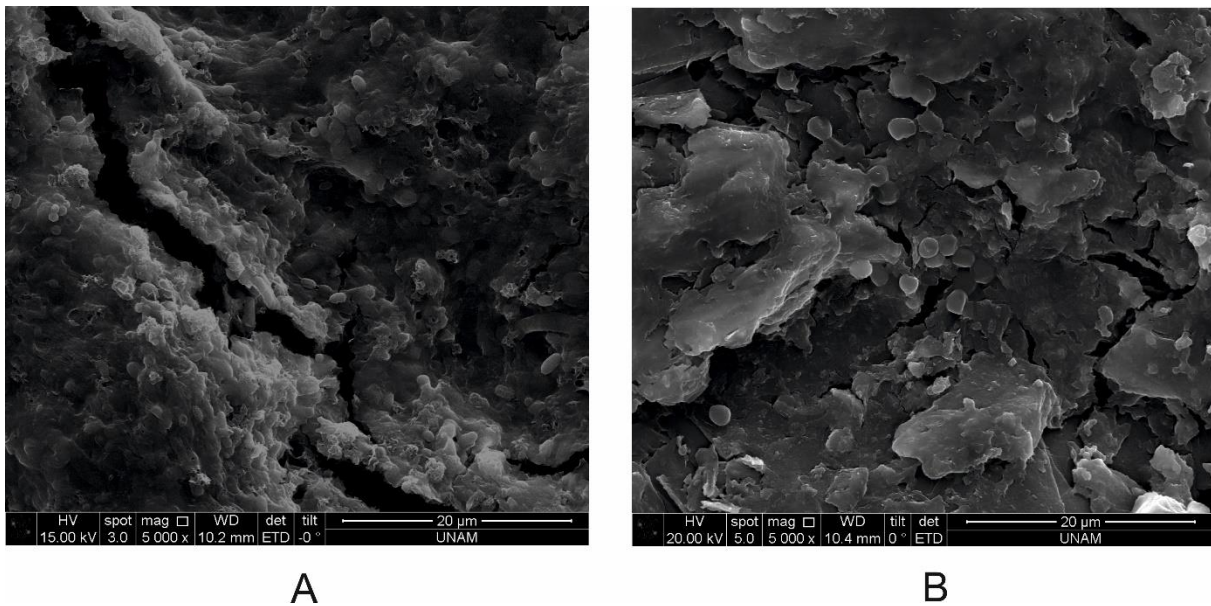


Figure 4. SEM images of biofilms on graphite electrodes of S-SMFC (A) and C-SMFC (B).

On the other hand, charged kinetics of the capacitors also showed that S-SMFC charged the capacitor faster than capacitors of C-SMFC in the hours, and the charged trends of S-SMFC was more stable than C-SMFC during the experiment period (Figure 3b). Correspondingly, R^2 values were recorded as 0,7028 and 0,635 for S-SMFC and C-SMFC, respectively. More importantly, the results from capacitors potential indicated that the bioelectricity was mostly generated first 12 hours, and then they charged small amount after 12 hours both in S-SMFC and C-SMFC. Therefore, it can be hypothesized that electrogenic bacteria populations in the reactors more active when the liquid organic waste dosing into reactor matrixes, and so the waste disposal was mostly related to bacterial population density.

3.3. Bacterial Analysis

Metagenomics analysis results for S-SMFC and C-SMFC are illustrated in Figure 5. It can be seen in Figure 5 that Proteobacteria was the higher population density both in S-SMFC and C-SMFC which were 54% for S-SMFC and 52% for C-SMFC among the other bacterial group. This is important because the electrogenic bacteria are categorized in proteobacteria group, and thus this phenomenon provided crucial evidences that electrogenic bacteria found in the reactor matrixes. Furthermore, Firmucutes which contains important electrogenic bacteria were also found high percent that 28% and 11% for S-SMFC and C-SMFC, respectively. On the other hand, the results showed that density of Proteobacteria and Firmucutes in S-SMFC were higher than those of C-SMFC, so it can be hypothesized that more current flow in the S-SMFC was lead to increasing electrogenic bacteria population. Increased population provided more organic matter treatment in the S-SMFC during the experiment period. This can be explained why S-SMFC was disposed more liquid organic waste according to C-SMFC. Similarly, it can be also hypothesis that external energy income (solar energy in this study) in a sediment microbial fuel cell system may increase organic matter decomposition speed, and so the manager has high bioelectricity production and treatment efficiency in their systems. Unfortunately, there is no information in literature about a hybrid system contain SMFC, thus it is not possible to make any comparisons.

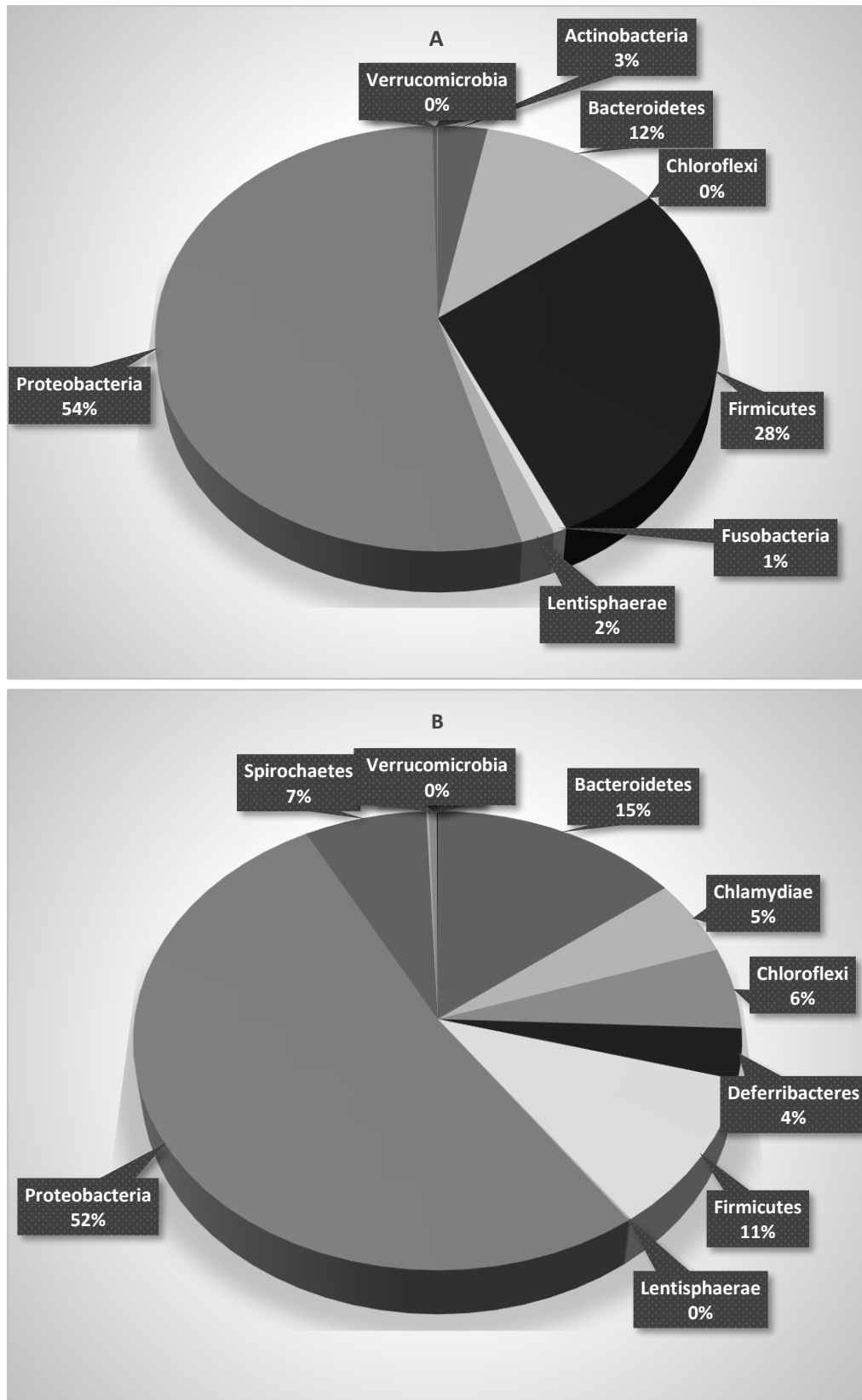


Figure 5. Metagenomics analysis results of S-SMFC (A) and C-SMFC (B)

The species composition both in S-SMFC and C-SMFC are given in Table 1. Correspondingly, *Azospirillum fermentarium* is the main species both in S-SMFC (41.26%) and C-SMFC (22.6%), and the other species ranged between 15.1% and 2.01%. *Azospirillum fermentarium* is commonly found in MFC devices and it is capable of organic matter decomposition and electron transfer. In this respect, various researchers are reported fermentation species in order to bioelectricity production by MFC devices. Chu et al. [20] reported *Azospirillum* species in a charged MFC. Yi et al. [21] found 21% *Azospirillum* content in a MFC used as biosensor. The other crucial species which determined in the present experiment were also reported in the MFC devices in order to bioelectricity production. The species is to *Clostridium sp.* [22], *Pseudomonas guangdongensis* [23], *Bacteroides sp.*[24], *Azovibrio restrictus* [25], *Levilinea saccharolytica* [26], *Seleniivibrio woodruffii* [27], *Geovibrio ferrireducens* [28].

Table 1. Species composition in S-SMFC and C-SMFC according to Metagenomics analysis results

S-SMFC		C-SMFC	
Species	Content (%)	Species	Content (%)
<i>Azospirillum fermentarium</i>	41.26	<i>Azospirillum fermentarium</i>	22.6
<i>Clostridium saccharoperbutylacetonicum</i>	15.1	<i>Pseudomonas guangdongensis</i>	10.37
<i>Azospirillum thiophilum</i>	5.85	<i>Sphaerochaeta associata</i>	6.64
<i>Bacteroides luti</i>	4.81	<i>Anoxybacillus thermanum</i>	6.62
<i>Magnetospirillum gryphiswaldense</i>	4.22	<i>Levilinea saccharolytica</i>	5.73
<i>Parabacteroides chartae</i>	3.07	<i>Lentimicrobium saccharophilum</i>	5.71
<i>Clostridium arbusti</i>	2.77	<i>Parachlamydia acanthamoebae</i>	5.34
<i>Clostridium pasteurianum</i>	2.15	<i>Parabacteroides chartae</i>	3.32
<i>Caproiciproducens galactitolivorans</i>	2.11	<i>Seleniivibrio woodruffii</i>	3.22
<i>Others*</i>	18.66	<i>Tistrella mobilis</i>	2.91
		<i>Meniscus glaucopsis</i>	2.57
		<i>Bdellovibrio bacteriovorus</i>	2.52
		<i>Azonexus hydrophilus</i>	2.18
		<i>Sulfurisoma sediminicola</i>	2.12
		<i>Azovibrio restrictus</i>	2.01
		<i>Others*</i>	16.15

4. CONCLUSIONS

In this study, a solar energy assisted sediment microbial fuel cell (S-SMFC) was evaluated bioelectricity production from liquid organic waste. Correspondingly, 840 mL liquid organic waste (10% juice waste and 10% sugary tea) was disposed by S-SMFC during the 60 days. The generated energy charged 100 F capacitor during the experiment period. More importantly, S-SMFC disposed more waste than control because S-SMFC has more electrogenic bacteria density (82%) compare to control (C-SMFC). Proteobacteria and Firmucutes provided crucial evidences to generate bioelectricity from liquid organic waste.

ACKNOWLEDGMENTS

This work was partly supported by the Scientific and Technological Research Council of Turkey (Project Code and Number: BİGG 1512-2200012). The author would like to thank to Prof. Dr. Cengiz TÜRE

(The Head of Ecology Section, Eskişehir Technical University, department of Biology and Dr. Anıl YAKAR (ECOWATT, Inc).

CONFLICT OF INTEREST

The author stated that there are no conflicts of interest regarding the publication of this article.

REFERENCES

- [1] Li H, Guo H, Huang N et al. Health risks of exposure to waste pollution: evidence from Beijing, China Economic Review, 2020; 63, 101540.
- [2] Shi Y, Deng Y, Wangn G et al. Stackelberg equilibrium-based eco-economic approach for sustainable development of kitchen waste disposal with subsidy policy: A case study from China, Energy, 2020; 196, 117071.
- [3] Kaiser J, Lerch M, Sedimentary faecal lipids as indicators of Baltic Sea sewage pollution and population growth since 1860 AD, Environmental Research, 2021; 112305.
- [4] Uğur A, Yılmaz OS, Çelen M, Ateş AM, Gülgen F, Şanlı FB. Determination of mucilage in the sea of marmara using remote sensing techniques with google earth engine, International Journal of Environment and Geoinformatics, 2021; 8, 423-434.
- [5] Yılmaz S, Küçüker MA, Kahraman D. Metagenomic characterization of planktonic communities during a mucilage event in the Çanakkale Strait (Dardanelles), Turkey, Journal of Anatolian Environmental and Animal Sciences, 2021; 6, 421-427.
- [6] Chun Y, Hua T, Anantharaman A et al. Organic matter removal from a membrane bioreactor effluent for reverse osmosis fouling mitigation by microgranular adsorptive filtration system, Desalination, 2021; 506, 115016.
- [7] Tałałaj LA, Bartkowska I, Biedka P. Treatment of young and stabilized landfill leachate by integrated sequencing batch reactor (SBR) and reverse osmosis (RO) process, Environmental Nanotechnology, Monitoring & Management, 2021; 16, 100502.
- [8] Chen W, Zhuo X, He C et al. Molecular investigation into the transformation of dissolved organic matter in mature landfill leachate during treatment in a combined membrane bioreactor-reverse osmosis process, Journal of Hazardous Materials, 2021; 397, 122759.
- [9] Türker OC. Simultaneous boron (B) removal and electricity generation from domestic wastewater using duckweed-based wastewater treatment reactors coupled with microbial fuel cell, Journal of Environmental Management, 2018; 228, 20-31.
- [10] Türker OC, Türe C, Yakar A, Saz Ç. Engineered wetland reactors with different media types to treat drinking water contaminated by boron (B), Journal of Cleaner Production, 2017; 168, 823-832.
- [11] Wang C, Jiang H. Real-time monitoring of sediment bulking through a multi-anode sediment microbial fuel cell as reliable biosensor, Science of The Total Environment, 2019; 697, 134009.

- [12] Prasad J, Tripathi, RK. Voltage control of sediment microbial fuel cell to power the AC load, *Journal of Power Sources*, 2020; 450, 227721.
- [13] Kabutey FT, Ding J, Zhao Q et al. Pollutant removal and bioelectricity generation from urban river sediment using a macrophyte cathode sediment microbial fuel cell (mSMFC), *Bioelectrochemistry*, 2019; 128, 241-251.
- [14] Neethu B, Ghangrekar M. Electricity generation through a photo sediment microbial fuel cell using algae at the cathode, *Water Science and Technology*, 2017; 76, 3269-3277.
- [15] Yang X, Chen S. Microorganisms in sediment microbial fuel cells: Ecological niche, microbial response, and environmental function, *Science of The Total Environment*, 2021; 756, 144145.
- [16] Rathour R, Patel D, Shaikh S et al. Eco-electrogenic treatment of dyestuff wastewater using constructed wetland-microbial fuel cell system with an evaluation of electrode-enriched microbial community structures, *Bioresource Technology*, 2019; 285, 121349.
- [17] Helder M. Design criteria for the plant-microbial fuel cell: electricity generation with living plants: from lab tot application, 2012.
- [18] Commault AS, Lear G, Packer MA et al. Weld, Influence of anode potentials on selection of *Geobacter* strains in microbial electrolysis cells, *Bioresource Technology*, 2013; 139, 226-234.
- [19] Kim JR, Cheng S, Oh SE et al. Power generation using different cation, anion, and ultrafiltration membranes in microbial fuel cells, *Environmental Science & Technology* 2007; 41, 1004-1009.
- [20] Chu N, Zhang L, Hao W et al. Rechargeable microbial fuel cell based on bidirectional extracellular electron transfer, *Bioresource Technology*, 2021; 329, 124887.
- [21] Yi Y, Xie B, Zhao T et al. Effect of external resistance on the sensitivity of microbial fuel cell biosensor for detection of different types of pollutants, *Bioelectrochemistry*, 2019; 125, 71-78.
- [22] Finch AS, Mackie TD, Sund CD et al. Metabolite analysis of *Clostridium acetobutylicum*: fermentation in a microbial fuel cell, *Bioresource Technology*, 2011; 102, 312-315.
- [23] Yang G, Han L, Wen J et al. *Pseudomonasguangdongensis* sp. nov., isolated from an electroactive biofilm, and emended description of the genus *Pseudomonas* Migula 1894, *International Journal of Systematic and Evolutionary Microbiology*, 2013; 63, 4599-4605.
- [24] Tang X, Qiao J, Chen C et al. Bacterial communities of polychlorinated biphenyls polluted soil around an e-waste recycling workshop, *Soil and Sediment Contamination: An International Journal*, 2013; 22, 562-573.
- [25] Suwanvitaya P, Boochoa S. Performance of Dairy Wastewater Intrinsic Bacteria in Microbial Fuel Cell, *Thai Environmental Engineering Journal*, 2021; 35, 43-52.
- [26] Lu L, Xing D, Ren ZJ. Microbial community structure accompanied with electricity production in a constructed wetland plant microbial fuel cell, *Bioresource Technology*, 2015; 195, 115-121.
- [27] Lin XQ, Li ZL, Liang B et al. Wang, Identification of biofilm formation and exoelectrogenic population structure and function with graphene/polyaniline modified anode in microbial fuel cell, *Chemosphere*, 2019; 219, 358-364.

- [28] Katuri KP, Enright AM, O'Flaherty V et al. Microbial analysis of anodic biofilm in a microbial fuel cell using slaughterhouse wastewater, *Bioelectrochemistry*, 2012; 87, 164-171.



RESEARCH ARTICLE

PREDICTING MYOCARDIAL INFARCTION COMPLICATIONS AND OUTCOMES WITH
DEEP LEARNING

İsmail Burak YAVRU ¹ , Sevcan YILMAZ GÜNDÜZ ² 

¹ Department of Electricity and Energy, Vocational School of Inegol, Bursa Uludag University, Bursa, Turkey

² Department of Computer Engineering, Faculty of Engineering, Eskişehir Technical University, Eskişehir, Turkey

ABSTRACT

Early diagnosis of cardiovascular diseases, which have high mortality rates all over the world, can save many lives. Various clinical findings and past histories of patients play an important role in diagnosing these diseases. These days, the prediction of cardiovascular diseases has gained great importance in the medical field. Pathological studies are prone to misinterpretation because too many findings are studied. For this reason, many automatic models that work with machine learning methods on patients' findings have been proposed. In this study, a model that predicts twelve myocardial infarction complications based on clinical findings is proposed. The proposed model is a deep learning model with three hidden layers with dropouts and a skip connection. A binary accuracy metric is used for measuring the performance of the proposed method. Rectified Linear Unit is set to the hidden layers and sigmoid function to the output layer as an activation function. Experiments were performed on a real dataset with 1700 patient records and carried out on two main scenarios; training on original data and training on augmented data with 100 epochs. As a result of the experiments, a total accuracy rate of 92% was achieved which is the best accuracy rate that has been proposed on this dataset.

Keywords: Deep Learning, Myocardial Infarction, Data Augmentation, Artificial Intelligence, Prediction

1. INTRODUCTION

Cardiovascular diseases (CVD) are one of the main reasons for death and disability in Europe. CVD reduce people's quality of life. Most deaths in Europe are due to CVD. In 2019, deaths from cardiovascular diseases in Europe accounted for 43% of total deaths [1]. Myocardial infarction (MI) is one of the most important cardiovascular pathological conditions [2].

Damage to the heart muscle occurs when blood flow is reduced or stopped. This damage leads to myocardial infarction or popularly known as heart attack. MI, a disease predominantly seen in developed countries, is becoming more common in developing countries. In proportion to the strong evidence base that cares for acute myocardial infarction is currently practiced records show a reduction in mortality [3-9]. Studies are showing that MI is preventable and curable. If a rapid recovery is not initiated, it can cause serious health problems and even death [18]. Therefore, early diagnosis of MI is very important. Early diagnosis can be achieved with various clinical findings and laboratory test results. Among these results, markers such as hypertension, diabetes, chronic heart disease, etc. play an important role in diagnosing MI [10-12]. Considering these values, myocardial infarction can be predicted and prevented.

Deep learning is a machine learning method based on artificial neural networks [12,13]. The deep neural networks (DNN) recognize the complex patterns of the test data given as inputs. A DNN aims to classify the outputs with high success, after a few epochs on the training data. [14]. Previous studies have shown that deep neural network methods have been used successfully for problems in the medical field. [15-

*Corresponding Author: burakyavru@uludag.edu.tr

Received: 12.01.2022

Published: 28.06.2022

17] The condition of applicants who might be classified as patients, could be predicted by training a deep neural network model on clinical features.

There are many input features in CVDs. These features are derived from the results of a series of laboratory results and medical imaging processes (ECG, etc.). In addition to these features, the patient's family history, medical history, risk factors, and physical examination findings can be counted. [18] We could predict the presence or absence of disease with statistical data containing these input features. The deep learning method could be trained with these inputs to predict the results and support the decision-making process of medical doctors.

There are several studies for predicting heart diseases with deep neural networks. One of the studies hired an autoencoder-based neural network for predicting heart disease [19]. This study consists of two parts. At the first stage, Moenye and friends trained an unsupervised neural network with a sparse autoencoder and at the second stage, they used an artificial neural network for prediction. The Heart Disease UCI dataset from Kaggle (<https://www.kaggle.com/ronitf/heart-disease-uci>, date of access is 09.01.2022) was used for this study. Several algorithm results were compared, as a result, they reached maximum 90% accuracy with the proposed method.

Another study aimed to predict coronary heart disease with convolutional neural networks. Dutta and friends trained and tested their approaches on data which is curated from National Health and Nutritional Examination Survey (NHANES) dataset. They propose a two-step approach: first for feature weight assessment and extracting important features. At the second step of the approach, they trained a fully connected layer and then classified tests. They had overall 79.5% accuracy with their proposed model [20].

Golovenkin et al. mentioned that the results of myocardial infarction may be too uneventful to be discovered even by experienced professionals, and they mentioned that the use of artificial neural networks in the diagnosis of this disease would be beneficial [24]. They used the “Myocardial infarction complications Database of University of Leicester” as a dataset [21] which is also used in this paper. They offered both 1 and 3 hidden layered ANN structures. The results they obtained with the model they proposed in their study have a total accuracy value of approximately 91.6%.

Study [22] was proposed by the same authors as study [24]. [22] was presented as a further study of [24] to predict more positive outcomes. Dorrer and friends aimed to predict the course of CVD with data augmentation. They used the same dataset [21] as in [24]. Due to the scarcity of positive output data, the authors proposed a data augmentation method and performed their testing on various deep neural network models. The authors had 72.14% total accuracy score from their final proposed model [22].

In this paper, we proposed an efficient deep neural network model for predicting MI complications and outcomes using the Myocardial infarction complications Database of the University of Leicester dataset. We performed our experiments both using augmented dataset and original dataset. All feature values in the dataset were trained and tested on all possible outcomes and complications. Results were compared with studies using the same dataset as in this study. The model optimized with adaptive moment estimation (Adam) algorithm, batch normalization, and dropout layers are also used against overfitting problem and improve performance. The proposed model in this study has better performance than the state-of-the-art literature approaches [19, 20, 22, 24].

2. MATERIALS AND METHODS

In this study, we used the Myocardial infarction complications database of the University of Leicester dataset to make our predictions [21]. This dataset has 1700 patients with MI. The database was collected in the Krasnoyarsk Interdistrict Clinical Hospital in Russia. The dataset has total 124 attributes. The first

112 attributes are about patients' clinical and laboratory data which were used as input features. The last 12 attributes hold the complications and outcomes information. The dataset has numerical and binary attributes. Most of the values consist of binary data. A total of 7.6% of data is missing in the database. The summary of complications and outcomes is presented in Table 1.

Table 1. The summary of complications and outcomes

Complication	Number of Cases	Fraction
Atrial fibrillation	170	10.0%
Supraventricular tachycardia	20	1.18%
Ventricular tachycardia	42	2.47%
Ventricular fibrillation	71	4.18%
Third-degree AV block	57	3.35%
Pulmonary edema	159	9.35%
Myocardial rupture	54	3.18%
Dressler syndrome	75	4.41%
Chronic heart failure	394	23.18%
Relapse of the MI	159	9.35%
Post-infarction angina	148	8.71%
Lethal outcome (cause) ¹	271	15.94%

¹Converted to binary attribute: dead or alive.

The gender distribution of the patients is 37% female and 63% male. Figure 1 shows the age and gender distribution. According to Figure 1, female patients admitted to the hospital with MI are older than male patients.

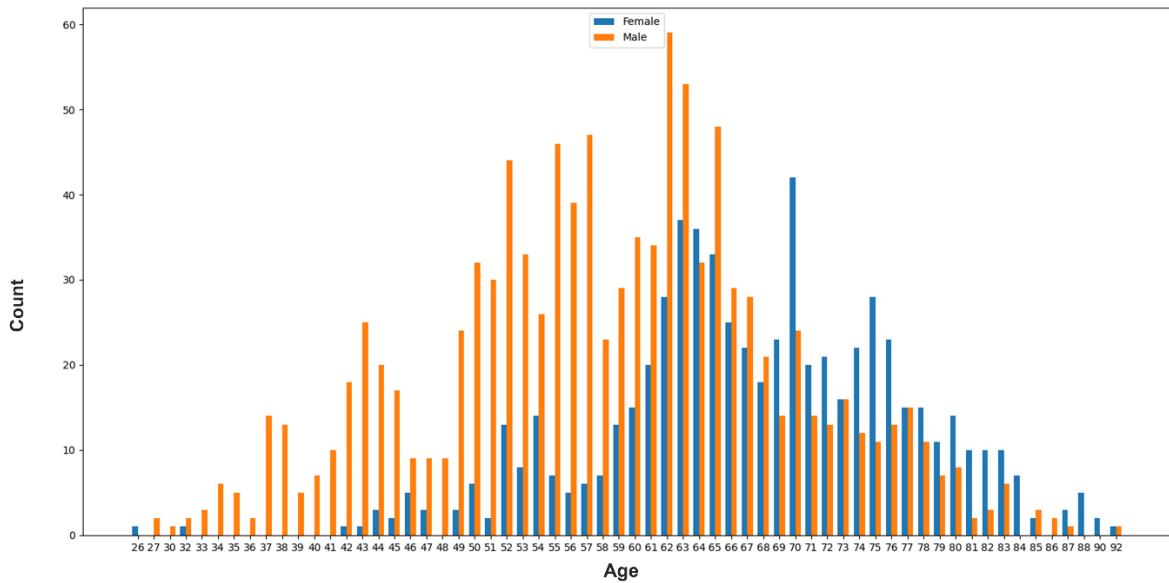


Figure 1. Age and Gender Distribution of dataset. (Blue bars – women, Orange bars – men)

Distributions of mortality depending on some important input features are shown in Figure 2.

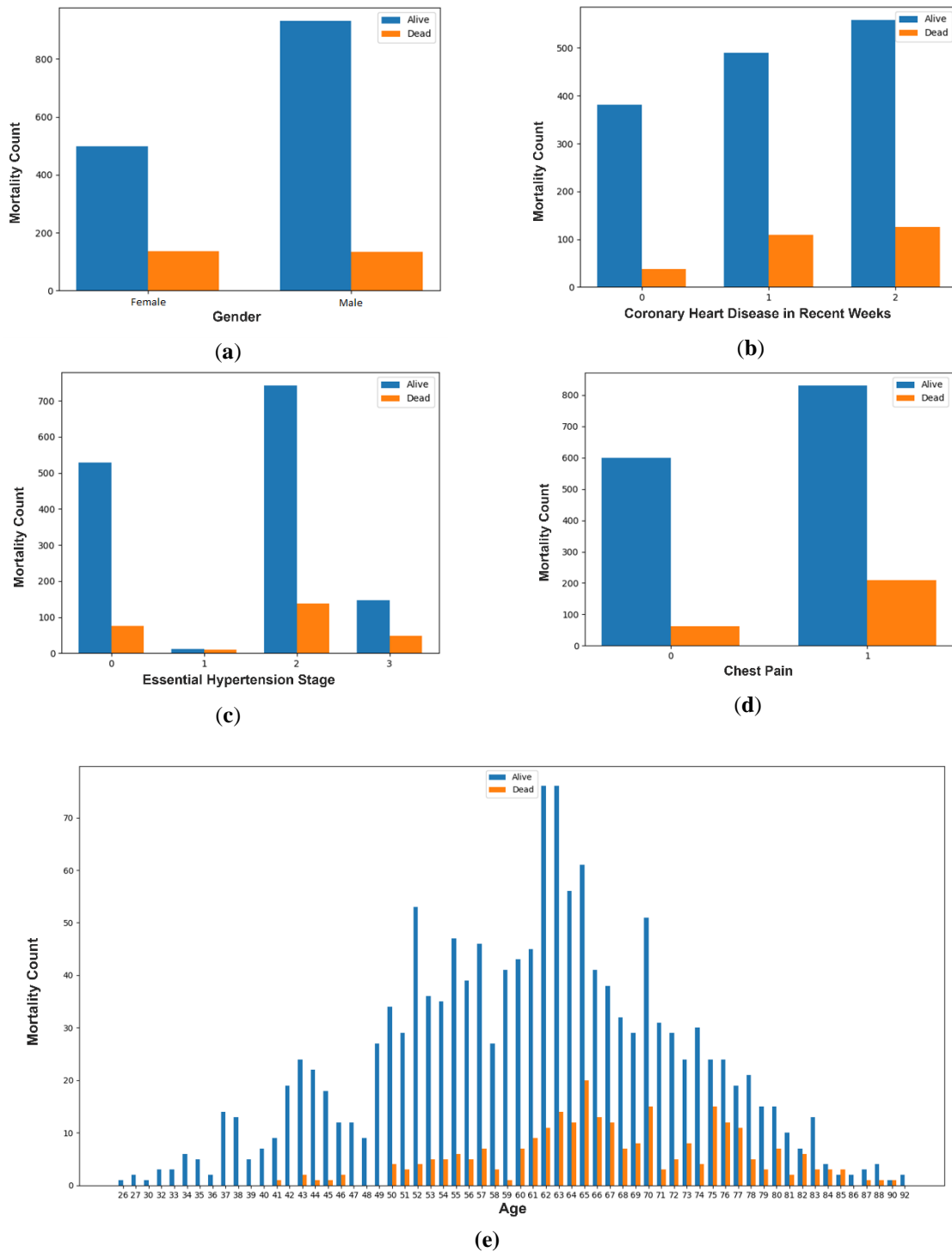


Figure 2. Distributions of mortality depending on some important input features: The blue bars indicate the number of deaths, and the orange bars indicate the number of lives.

Explanations of the charts in Figure 2 as follows; (a) Distribution of mortality rate according to gender; (b) Distribution of mortality rate according to coronary heart disease in recent weeks, days before hospital admission (0: There was no CHD, 1: Exertional angina pectoris, 2: Unstable angina pectoris); (c) Distribution of mortality rate according to essential hypertension (0: There is no essential hypertension, 1: Stage 1 Hypertension, 2: Stage 2 Hypertension, 3: Stage 3 Hypertension); (d)

Distribution of mortality rate according to exertional angina pectoris in the anamnesis (0: There is no chest pain,1: There is chest pain); (e) distribution of mortality rate by age.

Figure 2 (a) shows the number of female and male patients in terms of mortality rate. Although the number of male patients admitted to the hospital with MI is high, the mortality rate is higher in female patients. The number of patients with coronary heart disease (CHD) in the last weeks, days before hospital admission, is shown in Figure 2 (b). Patients with CHD before hospital admission have a higher mortality rate. Figure 2 (c) shows the mortality rate in terms of the presence of essential hypertension. Accordingly, applicants with 2nd and 3rd stage essential hypertension have a higher death count, but also without any essential hypertension, applicants are in the risk group. The number of patients who have exertional angina pectoris in the anamnesis is shown in Figure 2 (d) [23]. Chest pain due to coronary heart disease is called angina pectoris. It is an important sign for MI. The figure shows that patients with chest pain have a higher mortality rate. Figure 2 (e) presents the distribution of mortality rate by age. The death rate increases with age.

While carrying out this study, Keras, TensorFlow, and scikit-learn (sklearn) machine learning frameworks and numpy, pandas utility libraries were used in the Python development environment. The dataset was accessed from the University of Leicester website (https://leicester.figshare.com/articles/dataset/Myocardial_infarction_complications_Database/12045261?file=23581310, date of access is 09.01.2022). As mentioned above, there were some missing values. These missing values were filled with the mean of the attribute in which they were found. Lethal outcome (cause) (LET_IS) which is one of the important outcomes shows the patient is dead or alive after the hospital admission. LET_IS feature was a categorical attribute and it is converted to a binary attribute (0: Alive, 1: Dead) before calculations. After that, the first attribute of the dataset was dropped, which was patient ID.

All of the input features were transformed with sklearn's preprocessing method StandardScaler and then composed with the ColumnTransformer method. The proposed deep neural network architecture in this paper has three fully connected hidden layers with dropouts and a skip connection. The model is shown in Figure 3.

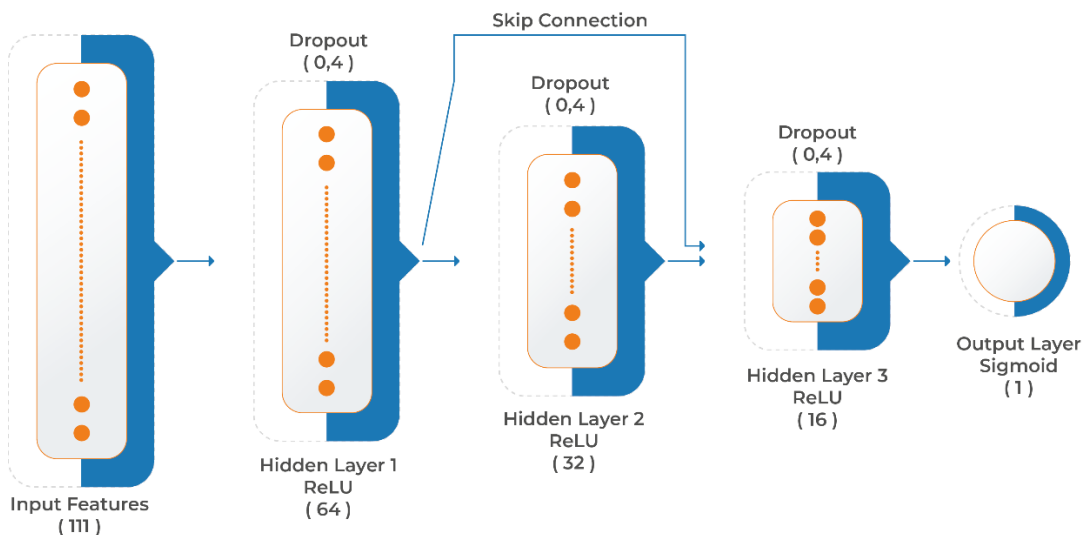


Figure 3. The proposed deep neural network architecture.

A dropout layer with a 0.4 rate was added after each hidden layer to prevent overfitting. Each hidden layer had Rectified Linear Unit (ReLU) as an activation function which is proposed in (1). x is a neuron input in (1).

$$f(x) = x^+ = \max(0, x) \tag{1}$$

If x is negative then the result will be zero, else whatever the input is, so is the output.

The training process was held through 100 epochs. However, it is known that if the number of epochs increases overfitting could occur, if the number of epochs decreases underfitting could occur. EarlyStopping API of Keras was hired to prevent overfitting and underfitting caused by epoch number. EarlyStopping API monitors validation loss value and stops the training when the model performance stops improving on the validation data. EarlyStopping API's parameters were as follows: monitor='val_loss', patience=5, restore_best_weights=True. EarlyStopper monitored validation loss with the patience of 5 epochs when the model performance stops improving. After stopping epochs, it restored the best weights.

The proposed deep neural network model also had a skip step. Skip step was originated from the first hidden layer to the third hidden layer. The third hidden layer took its inputs as a concatenation of the first and second layer's output. This skipping approach provided an uninterrupted gradient flow from the first layer to the third layer, which deals with the vanishing gradient problem. Concatenative skip connections, which were used in the proposed method, ensured the same size feature reusability from the first layer.

Sigmoid activation function was used at the output layer, shown in (2); where x_0 is the x value of the sigmoid's midpoint, L is the curve's maximum value and k is the logistic growth rate of the curve.

$$f(x) = \frac{L}{1 + e^{-k(x-x_0)}} \tag{2}$$

The Adam optimization algorithm was used to optimize the weight matrices and bias vectors. The default values provided by Keras for the Adam optimization algorithm ($\beta_1 = 0.9$, $\beta_2 = 0.999$, epsilon = None, decay = 0.0, amsgrad = False) have been preserved, just learning rate was modified as 0.0001. Binary cross entropy was used as a loss function. A binary accuracy metric function was used to judge the performance of the proposed model. Model parameters are proposed in Table 2.

Table 2. Deep neural network parameters.

Layer	Shape	Number of Parameters	Connected to
Input Layer	111	0	-
Hidden Layer 1	64	7168	Input Layer
Dropout Layer 1	64	0	Hidden Layer 1
Hidden Layer 2	32	2080	Dropout Layer 1
Dropout Layer 2	32	0	Hidden Layer 2
Concatenate	96	0	Hidden Layer 1, Dropout Layer 2
Hidden Layer 3	16	1552	Concatenate
Dropout Layer 3	16	0	Hidden Layer 3
Output Layer	1	17	Dropout Layer 3

The total trainable parameter count is 10.817 and the non-trainable parameter count is 0.

3. RESULTS AND DISCUSSION

The proposed architecture was evaluated on a PC with 2.9 GHz 4 core CPU, 8GB of memory, and without a GPU card. All experiments have been executed using PyCharm IDE with Python 3.8, Keras 2.7.0, and TensorFlow 2.7.0 on Windows 10 Pro x64.

Accuracy (3), Sensitivity (4), and Specificity (5) measures were used to assess the performance of the proposed method. Where, true positives (TP) were the number of cases correctly identified as sick or dead, false positives (FP) were the number of cases incorrectly identified as sick or dead, true negatives (TN) were the number of cases correctly identified as healthy or alive and false negatives (FN) were the number of cases incorrectly identified as healthy or alive.

$$Accuracy = \frac{TP + TN}{TP + TN + FP + FN} \times 100 \quad (3)$$

$$Specificity = \frac{TN}{TN + FP} \times 100 \quad (4)$$

$$Sensitivity = \frac{TP}{TP + FN} \times 100 \quad (5)$$

Experiments were handled in two main scenarios. In the first scenario, after the data preprocessing and model creation, the dataset was divided into three parts as training (60%), testing (20%), and validation (20%) data. The deep neural network model (DNN) was trained through 100 epochs. Our results and the results from the study [24] are presented in Table 3.

Table 3. First experiment results on complications and outcomes

Complication	Accuracy rates from our first scenario	Accuracy rates from [24]
Atrial fibrillation	90,85%	89,94%
Supraventricular tachycardia	98,53%	98,76%
Ventricular tachycardia	97,35%	97,47%
Ventricular fibrillation	96,67%	95,64%
Third-degree AV block	96,76%	96,59%
Pulmonary edema	90,29%	90,11%
Myocardial rupture	96,47%	96,70%
Dressler syndrome	96,17%	95,53%
Chronic heart failure	74,70%	75,57%
Relapse of the MI	87,64%	90,64%
Post-infarction angina	93,23%	91,23%
Lethal outcome (cause) ¹	86,47%	73,69%
Average	92,09%	90,98%

¹Converted to binary attribute: dead or alive.

As can be seen in Table 3, the average accuracy of our study was 92,09% which is slightly better than [24]. Total average specificity on all outcomes was 99,31% and total average sensitivity was just 4.09% in our study. It was very hard to predict true positive values due to the lack of positive outcomes. In study [24], authors made several experiments and had maximum 92,32% average specificity rate and there were no information about sensitivity rate.

In the second scenario, data was augmented as proposed in [22]. The main goal of the data augmentation was the augment the positive outcomes. The data augmentation process was handled instance by instance. The first instance was selected as an active instance and was extracted from the dataset. After

that, the instances with positive results in the data set were found. The number of positive instances was subtracted from the total number of instances and divided by the number of positive instances. Thus, the number of the count was found that how many times each positive instance would be duplicated in the dataset. After the data was copied to the end of the dataset, the DNN was retrained for each row. It was guaranteed that all copies of the relevant row were removed from the dataset before training to prevent the formation of bias. The augmentation structure is presented in Figure 4.

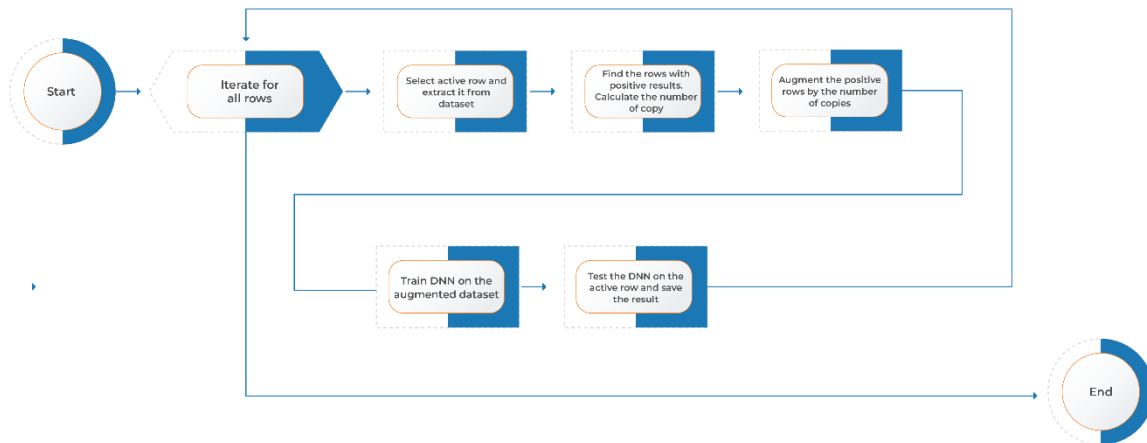


Figure 4. Data augmentation structure

Experiments results with the augmentation process are given in Table 4.

Table 4. Experiments results on the augmented dataset

Complication	Accuracy	Specificity	Sensitivity	Training Time in Seconds	Prediction Time in Seconds
Atrial fibrillation	71,79%	74,08%	51,17%	8082,45	93,13
Supraventricular tachycardia	89,04%	89,93%	10,00%	14872,19	93,42
Ventricular tachycardia	87,33%	89,13%	16,67%	12857,95	94,80
Ventricular fibrillation	82,27%	84,27%	36,62%	11433,16	99,66
Third-degree AV block	87,22%	89,09%	33,34%	12264,68	101,56
Pulmonary edema	76,20%	78,96%	49,36%	9386,78	95,47
Myocardial rupture	86,63%	88,44%	31,48%	12091,11	94,57
Dressler syndrome	80,04%	81,88%	40,00%	9850,98	95,78
Chronic heart failure	54,71%	53,83%	57,61%	3981,74	95,83
Relapse of the MI	66,49%	68,29%	49,06%	7251,57	96,53
Post-infarction angina	71,02%	72,96%	50,68%	7382,58	96,17
Lethal outcome (cause) ¹	76,38%	77,67%	69,51%	9318,83	94,63
Average	77,49%	79,71%	51,52%	118774,02	1151,55

¹Converted to binary attribute: dead or alive.

It was observed that the accuracy and specificity were decreased by the augmentation method. However, the number of positive outcome predictions was increased. In this way, the sensitivity value was increased approximately 11.6 times. Even if the accuracy and specificity were decreased with the presented method, it is clear that the results obtained in this study are more successful when compared to the results in [22]. Table 5 shows the results from [22] and the results presented in this study.

Table 5. First experiment results on complications and outcomes

Method	Overall Accuracy	Overall Precision	Overall Recall
Results in this study with 100 epochs	77,49%	17,88%	51,52%
Results in this study with 200 epochs	78,31%	18,68%	51,70%
Results from [22] with 100 epochs	72,14%	6,09%	29,57%
Results from [22] with 200 epochs	75,02%	5,86%	24,69%

As can be seen in Table 4, our overall accuracy result is 7.42% better with 100 epochs and 4.39% better with 200 epochs. Overall precision and recall are also 2.94 and 1.74 times better with 100 epoch and 3,19 and 2,09 times better with 200 epochs, respectively.

Differences between our model and the model proposed in [22] is given in Table 5.

Table 6. Differences between our model and the model proposed in [22]

Model Feature	Proposed in this study	Proposed in [22]
Activation Function on hidden layers	ReLU	Sigmoid
Optimizer	Adam	RMSProp
Metrics	Binary Accuracy	Accuracy
Dropout Rate	0.4	0.2
Skip Connection	Yes – From 1 st to 3 rd Hidden Layer	No

4. CONCLUSION

Coronary diseases affect people's quality of life. However, these diseases could be treated. One of the most important Coronary diseases is myocardial infarction. Early diagnosis is very important in such diseases. To make the diagnosis, the laboratory results, physical examination results, and ECG of the samples taken from the patients are evaluated.

In this study, it was tried to predict the diseases of the patients based on these types of values. Comparisons were made with the results obtained in previous studies. Results have improved when compared to previous studies. An average of 77.49% accuracy was achieved in the DNN architecture trained on the augmented dataset, and 92.08% accuracy was achieved in the DNN architecture trained with the original data set. Better results were obtained from the last study [22] working on the same dataset.

As presented in Table 3, the results of the first experiment were compared with the study in [24]. The model we presented in this study achieved better accuracy than the model presented in [24]. Compared with [24], this study showed obvious success on specificity values in the first scenario.

In the second scenario involving data augmentation, the effects of the model we proposed on accuracy, specificity and sensitivity were observed. Our proposed model has been tested in two stages, 100 epochs and 200 epochs. In both cases, more successful results were obtained than in [22], as presented in Table 5. Our proposed model achieved relatively better results at 200 epochs.

It has been observed that the skip connections between the first and third layers of our proposed DNN model, which prevents the loss of features, provide a better learning.

As further work, even more, successful results can be achieved by selecting input features that are considered more relevant (reducing the size of the input layer). In addition, separate models could be developed for each outcome and complication. Thus, more successful results can be obtained.

CONFLICT OF INTEREST

The authors stated that there are no conflicts of interest regarding the publication of this article.

REFERENCES

- [1] Timmis A, Townsend N, Gale CP, Torbica A, Lettino M, Petersen SE, Mossialos EA, Maggioni AP, Kazakiewicz D, May HT, et al. European Society of Cardiology: cardiovascular disease statistics 2019. *European heart journal*, 2020, 41.1: 12-85.
- [2] White HD, Chew DP. Acute myocardial infarction. *The Lancet*, 2008, 372.9638: 570-584.
- [3] Bassand JP, Hamm CW, Ardissino D, Boersma E, Budaj A, Fernández-Avilés F, Fox KAA, Hasdai D, Ohman RM, Wallentin L, Wijns W, et al. Guidelines for the diagnosis and treatment of non-ST-segment elevation acute coronary syndromes: The Task Force for the Diagnosis and Treatment of Non-ST-Segment Elevation Acute Coronary Syndromes of the European Society of Cardiology. *European heart journal*, 2007, 28.13: 1598-1660.
- [4] Anderson JL, Adams CD, Antman EM, Bridges CR, Califf RM, Casey DE, Chavey WE, Fesmire FM, Hochman JS, Levin TN, et al. ACC/AHA 2007 guidelines for the management of patients with unstable angina/non–ST-elevation myocardial infarction, *Journal of the American College of Cardiology*, 2007, 50.7: e1-e157.
- [5] Fox KAA, Steg FG, Eagle KA, Goodman SG, Anderson FA, Granger CB, Flather MD, Budaj A, Quill A, Gore JM. Decline in rates of death and heart failure in acute coronary syndromes, 1999-2006. *Jama*, 2007, 297.17: 1892-1900.
- [6] Furman MI, Dauerman HL, Goldberg RJ, Yarzbeski J, Lessard D, & Gore JM. Twenty-two year (1975 to 1997) trends in the incidence, in-hospital and long-term case fatality rates from initial Q-wave and non-Q-wave myocardial infarction: a multi-hospital, community-wide perspective. *Journal of the American College of Cardiology*, 2001, 37.6: 1571-1580..
- [7] Mandelzweig L, Battler A, Boyko V, Bueno H, Danchin N, Filippatos G, Gitt A, Hasdai D, Hasin Y, Marrugat J, et al. The second Euro Heart Survey on acute coronary syndromes: characteristics, treatment, and outcome of patients with ACS in Europe and the Mediterranean Basin in 2004. *European heart journal*, 2006, 27.19: 2285-2293.
- [8] Liew R, Sulfi S, Ranjadayalan K, Cooper J, Timmis AD. Declining case fatality rates for acute myocardial infarction in South Asian and white patients in the past 15 years. *Heart*, 2006, 92.8: 1030-1034.
- [9] Jaffe AS, Babuin L, Apple FS. Biomarkers in acute cardiac disease: the present and the future. *Journal of the American college of cardiology*, 2006, 48.1: 1-11.
- [10] Antman EM, Cohen M, Bernink PJ, McCabe CH, Horacek T, Papuchis G, Mautner B, Corbalan R, Radley D, Braunwald E. The TIMI risk score for unstable angina/non–ST elevation MI: a method for prognostication and therapeutic decision making. *Jama*, 2000, 284.7: 835-842.
- [11] Granger CB, Goldberg RJ, Dabbous O, Pieper KS, Eagle KA, Cannon CP, Werf F, Avezum A, Goodman SG, Flather MD, et al. Predictors of hospital mortality in the global registry of acute coronary events. *Archives of internal medicine*, 2003, 163.19: 2345-2353.

- [12] Huang Y, Wu Z, Wang L, Tan T. Feature coding in image classification: A comprehensive study. *IEEE transactions on pattern analysis and machine intelligence*, 2013, 36.3: 493-506.
- [13] Schmidhuber J. Deep learning in neural networks: An overview. *Neural networks*, 2015, 61: 85-117.
- [14] LeCun Y, Bengio Y, Hinton G. Deep learning. *nature*, 2015, 521.7553: 436-444.
- [15] Min S, Lee B, Yoon S. Deep learning in bioinformatics. *Briefings in bioinformatics*, 2017, 18.5: 851-869.
- [16] Angermueller C, Pärnamaa T, Parts L, Stegl O. Deep learning for computational biology. *Molecular systems biology*, 2016, 12.7: 878.
- [17] Ching T, Himmelstein DS, Beaulieu-Jones BK, Kalinin AA, Do BT, Way GP, Ferrero E, Agapow PM, Zietz M, Hoffman MM, et al. Opportunities and obstacles for deep learning in biology and medicine. *Journal of The Royal Society Interface*, 2018, 15.141: 20170387.
- [18] Swathy M, Saruladha KA. comparative study of classification and prediction of Cardio-Vascular Diseases (CVD) using Machine Learning and Deep Learning techniques. *ICT Express*, 2021.
- [19] Mienye ID, Sun Y, Wang Z. Improved sparse autoencoder based artificial neural network approach for prediction of heart disease. *Informatics in Medicine Unlocked*, 2020, 18: 100307.
- [20] Dutta A, Batabyal T, Basu M, Acton ST. An efficient convolutional neural network for coronary heart disease prediction. *Expert Systems with Applications*, 2020, 159: 113408.
- [21] Golovenkin SE. Myocardial infarction complications Database. University of Leicester, 2020.
- [22] Dorrer MG, Golovenkin SE, Nikulina SY, Orlova YV, Pelipeckaya EY, Vereshchagina TD. Selection of neural network architecture and data augmentation procedures for predicting the course of cardiovascular diseases. In: *Journal of Physics: Conference Series*. IOP Publishing, 2021. p. 032037.
- [23] Yasue H, Omote S, Takizawa A, Nagao M, Miwa K, Tanaka S. Exertional angina pectoris caused by coronary arterial spasm: effects of various drugs. *The American journal of cardiology*, 1979, 43.3: 647-652.
- [24] Golovenkin SE, Dorrer MG, Nikulina SY, Orlova YV, Pelipeckaya EY. Evaluation of the effectiveness of using artificial intelligence to predict the response of the human body to cardiovascular diseases. *The American journal of cardiology, Journal of Physics: Conference Series*, 2020, 1679: 042017